Beyond BioID: Streptavidin outcompetes antibody fluorescence signals in protein localization and readily visualises targets evading immunofluorescence detection

Johanna Odenwald[1], Bernardo Gabiatti[1], Silke Braune[1], Siqi Shen[2], Martin Zoltner[2*] and Susanne Kramer[1*]

[1] Biocenter, University of Würzburg, Würzburg, Germany

[2] Department of Parasitology, Faculty of Science, Charles University in Prague, Biocev, Vestec, Prague, Czech Republic

* corresponding authors

Tel.: +49 931 3186785

Email: susanne.kramer@uni-wuerzburg.de

Email: martin.zoltner@natur.cuni.cz

short title: Imaging applications of TurboID

ABSTRACT

Immunofluorescence is a common method to localise proteins within their cellular context via fluorophore labelled antibodies and for some applications without alternative. However, some protein targets evade detection due to low protein abundance or accessibility issues. In addition, some imaging methods require a massive reduction in antigen density thus impeding detection of even medium-abundant proteins.

Here, we show that the fusion of the target protein to TurboID, a biotin ligase labelling lysine residues in close proximity, and subsequent detection of biotinylation by fluorescent streptavidin offers an “all in one” solution to the above-mentioned restrictions. For a wide range of target proteins tested, the streptavidin signal was significantly stronger than an antibody signal, markedly improving the imaging sensitivity in expansion microscopy and correlative light and electron microscopy, with no loss in resolution. Importantly, proteins within phase-separated regions, such as the central channel of the nuclear pores, the nucleolus or RNA granules, were readily detected with streptavidin, while most antibodies fail to label proteins in these environments. When TurboID is used in tandem with an HA epitope tag, co-probing with streptavidin and anti-HA can be used to map antibody-accessibility to certain cellular regions. As a proof of principle, we mapped antibody access to all trypanosome nuclear pore proteins (NUPs) and found restricted antibody labelling of all FG NUPs of the central channel that are known to be phase-separated, while most non-FG Nups could be labelled. Lastly, we show that streptavidin imaging can resolve dynamic, temporally and spatially distinct sub-complexes and, in specific cases, reveal a history of dynamic protein interaction.

In conclusion, streptavidin imaging has major advantages for the detection of lowly abundant or inaccessible proteins and in addition, can provide information on protein interactions and biophysical environment.

INTRODUCTION

Visualisation of a protein within the cellular context is routinely achieved either by fusing it to a fluorescent protein, or by using fluorophore labelled antibodies specific for a target protein or peptide tag that is genetically fused to it. Fluorescent proteins are not suitable for all imaging applications, because fluorescence is lost under fixation and permeabilization conditions. Applications that are fully dependent on antibodies include correlative electron and light microscopy (CLEM) applications, expansion microscopy or protein detection in combination with *in situ* hybridisation for nucleic acid detection.

Sometimes, antibodies fail to detect a protein at its expected localisation, which is rarely followed up or reported. We recently observed the absence of an anti-HA antibody signal at the nuclear pores for endogenously expressed trypanosome mRNA export factor MEX67 fused to the small peptide hemagglutinin (HA) epitope tag: the anti-HA signal was entirely restricted to the nucleoplasm (Moreira et al., 2023). Likewise, a polyclonal antibody raised against *T. brucei* MEX67 did not stain the nuclear pores (Pozzi et al., 2023). In contrast, fusions of *T. brucei* MEX67 to fluorescent proteins (either N- or C-terminally) are primarily detected at the nuclear pores with some signal extending to the nucleoplasm (Billington et al., 2023; Kramer et al., 2010). This is in agreement with the reported function of *T. brucei* MEX67 in mRNA export (Dostalova et al., 2013; Schwede et al., 2009) and with nuclear pore localisation of MEX67 orthologues in other eukaryotes (Katahira et al., 1999; Köhler and Hurt, 2007; Mangus et al., 2003; Rodriguez et al., 2004; Stewart, 2019; Sträßer et al., 2000; Terry and Wente, 2007) where Mex67 was even termed a mobile nucleoporin (Derrer et al., 2019).

We next expressed *Tb*MEX67 fused to a TurboID-HA tandem tag. TurboID is a biotin ligase, widely employed for proximity labelling techniques facilitating analysis of protein interactions *in vivo* (Branon et al., 2018). To our surprise, fluorophore labelled streptavidin readily delivered a signal localizing primarily to the nuclear pores and partially to the nucleoplasm, consistent with the localisation of MEX67 fused to fluorescent proteins (Moreira et al., 2023). We therefore concluded that the streptavidin signal shows the correct localization of MEX67, while antibodies fail to bind MEX67 at the nuclear pore and selectively stain the nucleoplasmic fraction of MEX67. One possible reason for the absence

79 of antibody stain could be the localisation of MEX67 to the central channel of the nuclear
80 pore that is lined by phenylalanine-glycine nucleoporins (FG NUPs), intrinsically disordered
81 proteins dominated by FG-repeats, that assemble to a dense meshwork and create a phase-
82 separated environment, physically distinct from the rest of the cell (Davis et al., 2022; Nag et
83 al., 2022). It remains unclear, why streptavidin was able to stain biotinylated proteins within
84 these antibody inaccessible regions, but possible reasons are: (i) tetrameric streptavidin is
85 smaller and more compact than IgGs (60 kDa versus a tandem of two IgGs, each with 150
86 kDa) (ii) the interaction between streptavidin and biotin is ~100 fold stronger than a typical
87 interaction between antibody and antigen and (iii) streptavidin contains four fluorophores,
88 in contrast to only one per secondary IgG.
89
90 Here, we set out to investigate whether streptavidin imaging offers a general solution to
91 antibody-accessibility problems. We expressed 11 trypanosome and one mammalian protein
92 of different *bona fide* phase-separated regions (nucleolus, stress granules, central channel of
93 the nuclear pores) fused to a TurboID-HA tandem tag. All proteins could be readily visualised
94 with streptavidin, while they could not be labelled with anti-HA. Importantly, we noticed
95 that streptavidin imaging has further major advantages to antibody labelling, even for
96 antibody-accessible proteins: (i) the multiple biotinylation sites of the bait and adjacent
97 proteins provided a massive boost in signal, which is in particular useful in applications with
98 diluted antigens, such as expansion microscopy or correlative light and electron microscopy
99 (CLEM); (ii) since biotinylation extends to adjacent proteins and is stable over the lifetime of
100 a protein, protein interactions are preserved in time, enabling to monitor dynamic processes
101 in the cell.

102 **MATERIALS and METHODS**

103

104 *Culture and genetic modification of trypanosomes*

105 *T. b. brucei* Lister 427 procyclic cells were cultured in SDM-79 (Brun and Schönenberger,
106 1979). Generation of transgenic trypanosomes was performed using standard methods
107 (McCulloch et al., 2004). Almost all trypanosome fusion proteins were expressed from the
108 endogenous locus, by modifying one allele via a PCR-based approach reliant on a (modified)
109 version of the pPOT vector system (Dean et al., 2015). Occasionally, a plasmid-based system
110 was used for endogenous tagging (Kelly et al., 2007). For overexpression of ALPH1-eYFP, a
111 tetracycline inducible system was used (Sunter et al., 2012) and expression was induced for
112 24 hours. Details about all fusion constructs are provided in Table S1. The TurboID-HA
113 tandem tag encodes the TurboID open reading frame, followed by a two-amino acid long
114 spacer (AS), followed by the HA tag (YPYDVPDYA). The TurboID-Ty1 tandem tag encodes the
115 TurboID open reading frame, followed by a short linker (ASGSGS), followed by the Ty1 tag
116 (EVHTNQDPLD).

117

118 *Culture and genetic manipulation of HeLa cells*

119 pEGFP-N1 was modified to contain the sequence encoding TurboID-4HA with a stop-codon
120 upstream of the eGFP sequence. Sequences of the open reading frames of NUP88 and
121 NUP54 were amplified from human cDNA and cloned in frame downstream of the TurboID-
122 4HA sequence. This results in expression of NUP88 or NUP54 fused to the N-terminal
123 TurboID-4HA tag, without the eGFP. The sequences of the fusion proteins are provided in
124 Table S1. HeLa cells were grown in Dulbecco's modified Eagle's medium (DMEM; Gibco by
125 Life Technologies, Darmstadt, Germany) supplemented with 10% fetal calf serum (FCS;
126 Capricorn Scientific, Ebsdorfergrund, Germany) and 1% penicillin-streptomycin (Thermo
127 Fisher Scientific, Dreireich, Germany) at 37°C and 5% CO_2. Cells were transfected with the
128 respective TurboID-HA fusion constructs using Effectene™ (Qiagen, Hilden, Germany)
129 following the manufacturer's protocol and incubated for ~24 hours in a petri-dish containing
130 a coverslip. Immunofluorescence/streptavidin labelling was performed on cells attached to
131 the coverslips, as detailed below for trypanosomes.

132

133 *Immunofluorescence and streptavidin labelling*

About 1 × 10^7 procyclic-form *T. brucei* cells, harvested at a density of 5 × 10^6 cells/ml, were washed once in 1 ml SDM79 without hemin and serum and resuspended in 500 µl PBS. For fixation, 500 µl of 8% paraformaldehyde was added for 20 min while rotating. After addition of 7 ml PBS supplemented with 20 mM glycine, cells were pelleted, resuspended in 150 µl PBS, and spread on poly-lysine-coated slides (within circles drawn with a hydrophobic pen). Cells were allowed to settle for 15 min, before removing surplus PBS and permeabilizing cells with 0.5% Triton X-100 in PBS. Slides were rinsed in PBS, and cells were then blocked in 3% bovine serum albumin (BSA) in PBS for 30 min, followed by 60 min incubation with rabbit mAb-anti-HA C29F4 (1:500 dilution; Cell Signaling Technology) and Streptavidin-Cy3 (1:200 dilution; Jackson Laboratories) in PBS/3% BSA. Slides were washed in PBS (three times for 5 min), then incubated with anti-rabbit Alexa Fluor Plus 488 (1:500 dilution, A32731 Invitrogen) in PBS/3% BSA for 50 min and a further 10 min upon addition of 4',6-diamidino-2-phenylindole (DAPI) (0.1 µg/ml). Slides were washed 3 × 5 min in PBS and embedded into ProLong Diamond Antifade Mountant (Thermo Fisher Scientific). For control experiments, the following antibodies/nanobodies were used: Ty1-tag monoclonal antibody BB2 (hybridoma supernatant, 1:300); *T. brucei* MEX67 polyclonal antiserum (1:1000, kind gift of Mark Carrington) and anti-GFP nanobody (GFP-Booster Alexa Fluor 647 Chromotek gb2AF647, 1:1000).

Microscopy

For most fluorescence microscopy experiments, images were acquired using a DMI8 widefield microscope (Thunder Imager, Leica Microsystems, Germany) with a HCX PL APO CS objective (100x, NA = 1.4, Leica Microsystems) and Type F Immersion Oil (refractive index = 1.518, Leica Microsystems). The microscope was controlled using LAS-X software (Leica Microsystems). Samples were illuminated with an LED8 light source (Leica). Excitation light was selected by using the following filter sets: Ex 391/32 nm; DC 415nm; Em 435/30 nm (DAPI), 436/28 nm; DC 459 nm; Em 519/25 nm (AlexaFluor™ 488), 554/24 nm; DC 572 nm; Em 594/32 nm (Cy3), 578/24 nm; DC 598 nm; Em 641/78 nm (AlexaFluor™ 594). Images were captured using a K5 sCMOS camera (Leica, 6.5 µm pixel size). Between 50 and 70 images in 140 nm distances were recorded for each Z-stack. Exposure times were 100-200 ms for DAPI and between 200-800 ms for all other fluorophores. For some images, an inverted wide-field microscope Leica DMI6000B (Leica Microsystems GmbH, Wetzlar, Germany) equipped with a 100x oil immersion objective (NA 1.4) and a Leica

167 DFC365 camera (6.5 µm/pixel) was used. Filter sets were (i) ex: 340–380 nm, dc: 400nm, em:
168 450–490 nm (DAPI), (ii) ex: 450–490 nm, dc: 495nm, em: 500–550 nm (eYFP), (iii) ex: 530–
169 560nm, dc: 570 nm, em: 572- 648 nm (TMR). Image acquisition was done like on the
170 thunder imager. Images are shown either unprocessed (raw data) or processed by instant
171 computational clearing (Software provided by the Thunder imager) or deconvolution using
172 Huygens Essential software (Scientific Volume Imaging BV). Presentations are either as single
173 plane or as Z-stack projection (sum slices), as indicated. Scanning electron microscopy and
174 correlation with light microscopy was done as previously described (Kramer et al., 2020).
175
176 *Affinity enrichment of biotinylated proteins and on beads digestion*
177 The isolation of biotinylated proteins from trypanosomes and preparation for mass
178 spectrometry was done as previously described (Moreira et al., 2023), except that 1 mM
179 biotin was added during the elution step from the streptavidin beads by tryptic digest, to
180 improve recovery of biotinylated peptides.
181
182 *Western blots*
183 Western blotting was performed using standard methods. Detection of biotinylated proteins
184 was done with Streptavidin-IRDye®680LT (LI-COR) (1:20,000). Proteins with HA-tag(s) were
185 detected using rat mAb-anti-HA 3F10 (Roche, 1:1000) as primary antibody and
186 IRDye® 800CW Goat anti-Rat IgG (Licor, 1:20,000) as secondary antibody.
187
188 *Mass spectrometry and proteomics analysis*
189 TurboID-eluted peptides were resuspended in 50 mM NH_4HCO_3 and passed over C18 stage
190 tip columns as described (Rappsilber et al., 2007) and then analyzed by LC–MS/MS on an
191 Ultimate3000 nano rapid separation LC system (Dionex) coupled to an LTQ Orbitrap Fusion
192 mass spectrometer (Thermo Fisher Scientific). Minimum peptide length was set at seven
193 amino acids allowing a maximum of two missed cleavages, and FDRs of 0.01 were calculated
194 at the levels of peptides, proteins, and modification sites based on the number of hits
195 against the reversed sequence database. Spectra were processed using the intensity-based
196 label-free quantification (LFQ) in MaxQuant version 2.1.3.0 (Cox and Mann, 2008; Cox et al.,
197 2014) searching the *T. brucei* strain TREU927 annotated protein database (version 63) from
198 TriTrypDB (Aslett et al., 2010). Statistical analyses of LFQ data were done in Perseus (Tyanova

199 et al., 2016). LFQ values were filtered for at least one valid value in the bait sample group,
200 log2 transformed and missing values imputed from a normal distribution of intensities
201 around the detection limit of the mass spectrometer. These values were subjected to a
202 Student's t-test comparing the respective bait sample groups to an untagged control (wt
203 parental cells) triplicate sample group. The resulting *t*-test difference is the difference
204 between the means of logarithmic abundances of a protein group. Bait samples were
205 prepared in duplicate (NUP76, NUP96, NUP110) or triplicate (MEX67, NUP158). All
206 proteomics data have been deposited at the ProteomeXchange Consortium via the PRIDE
207 partner repository (Perez-Riverol et al., 2019) with the dataset identifier PXD031245
208 (MEX67, NUP158, wt control, GFP control) and PXD047268 (NUP76, NUP96, NUP110).
209
210 *Ultrastructural Expansion Microscopy (U-ExM) with procyclic T. brucei*
211 The U-ExM method was performed as described in (Gambarotto et al., 2020) with some
212 modifications. $1x10^7$ trypanosome cells were harvested (1500 g, 10 min) and the pellet
213 resuspended in 500 µl PBS. 500 µl 8% formaldehyde (FA, 36.5-38%, F8775, Sigma)/8%
214 acrylamide (AA, 40%, A4058, Sigma) diluted in PBS was added to achieve a final
215 concentration of 4%FA/4%AA. Cells were allowed to settle on a 12 mm round coverslip
216 treated with poly-L-lysine (P8920, Sigma) placed in a well of a 24-well plate. The adjacent
217 wells were filled with ddH_2O, the plate sealed with parafilm and incubated at 37°C for 5
218 hours. A small piece of parafilm was placed on top of a humid chamber, where a drop of
219 monomer solution (sodium acrylate 23% (w/v) (408220, Sigma), AA 10% (w/v), N-N'-
220 methylenebisacrylamide 0.1% (w/v) (M7279, Sigma) in PBS) was added. The coverslip was
221 placed on top of the drop, with the cells facing down. The coverslip was removed, cleaned
222 from excess liquid with a laboratory wipe and placed in 40 µl of monomer solution freshly
223 complemented with 1 µl 10% APS (327085000, Acros Organic) and 1 µl 10% TEMED (T7024,
224 Sigma). Sodium acrylate stock solution 38% (w/v) was prepared by dissolving 1.9 g sodium
225 acrylate in 3.1 ml of ddH_2O followed by filtering through 0.2 µm filter. The humid chamber
226 was closed, and the gel allowed to polymerize for one hour at 37°C. Coverslips were
227 transferred to a well of a 6-well plate containing 1 ml denaturation buffer (200 mM SDS
228 (A1112, Applichem), 200 mM NaCl (A2942, Applichem) and Tris-HCl pH 9 (5429.3, Roth)) and
229 incubated for 15 minutes with gentle shaking. Gels were detached from the coverslips with a
230 spatula and transferred to a 1.5 mL Eppendorf tube. The tube was filled with denaturation

231 buffer to the top, closed and incubated at 95°C for 90 minutes in a heating block. Gels were
232 transferred to a beaker with 100 ml ddH_2O for the first round of expansion for 30 minutes.
233 Water was exchanged and two more rounds of expansion were done, the last one being
234 overnight at room temperature. The next day, gels were carefully transferred to a Petri dish
235 and imaged to measure the expansion factor. Gels were transferred to a fresh beaker
236 containing 100 ml PBS and incubated for 15 minutes. This was repeated once and then the
237 gel was trimmed to a square of about 12 x 12 mm which was transferred to a 24-well plate
238 for antibody incubation. Gels were incubated with 0.5 ml PBS BSA 3% (A1391, Applichem)
239 with primary antibodies (mouse-anti-HA monoclonal antibodies (C29F4, Cell Signaling) at
240 1:500) at 37°C for three hours in a plate shaker at 1500 RPM. Gels were transferred to a 6-
241 well plate for washing. They were washed three times with 10 ml PBS-T (0.1% Tween20 in
242 PBS) for 10 minutes with agitation at room temperature. Gels were transferred back to a 24-
243 well plate and incubated with 0.5 ml PBS BSA 3% with secondary antibodies AlexaFluor™ 488
244 goat anti-rabbit (A11008, Sigma, 1:500), Cy3-streptavidin and 0.1 µg/ml DAPI (D9542, Sigma)
245 at 37°C for three hours in a plate shaker at 1500 RPM. Gels were transferred to the 6-well
246 plate and washed four times with 10 ml PBS-T for 10 minutes with agitation at room
247 temperature, all steps from now on protected from light. Gel pieces were expanded again in
248 100 ml ddH_2O in a beaker, with three water exchanges each 30 minutes and the last
249 expansion step done overnight at room temperature. An imaging chamber Nunc™ Lab-Tek™
250 II with one chamber (734-2055, Thermofisher Scientific) was covered with a layer of poly-D-
251 lysine (A3890401, Gibco) for one hour and left to dry overnight. For imaging, the gel pieces
252 were trimmed to fit the chamber, excess water was removed with a laboratory wipe and the
253 gel was placed in the imaging chamber, taking care not to shift after the initial placement. A
254 drop of water was added to cover the top of the gel. The gel chamber was closed with the lid
255 to avoid evaporation during imaging. For longer imaging sessions, drops of water were
256 periodically added to prevent gel drying. Since cells can be on either side of the gel, the gel
257 was divided into two pieces, one facing up and one facing down, to ensure cells can be
258 detected, on either piece.
259
260 *Protein retention Expansion Microscopy (proExM) in procyclic T. brucei*
261 The proExM method was performed as described in (Tillberg et al., 2016) with some
262 modifications. $5x10^7$ cells were harvested by centrifugation at 1500 g for 10 minutes,

263 washed once in 10 ml PBS and finally resuspended in 1 ml of PBS. 1 ml of PFA 8% (P6148,
264 Sigma) was added and cells were fixed for 20 minutes at room temperature with rotation. 13
265 ml 20 mM glycine (50046, Sigma) in PBS (freshly prepared from a 2M stock) was added to
266 quench and cells were harvested at 1500 g for 10 minutes. Cells were resuspended in 1 ml
267 PBS and let to adhere to a 12 mm coverslip, previously treated with poly-L-lysine, placed in a
268 well of a 24 well plate for 15 minutes. The well was rinsed with PBS and the coverslip
269 incubated with PBS 0.5% Triton for 5 minutes for permeabilization. Wells were rinsed again
270 with PBS and coverslips incubated with PBS 3% BSA for 30 minutes for blocking. 50 µl of
271 primary antibody solution (rabbit anti-HA monoclonal antibodies (C29F4, Cell Signaling) 1:50
272 diluted in PBS BSA 1%) were placed on a piece of parafilm in a humid chamber and the cover
273 slip was placed on top (cells facing down) for one hour in a humid chamber. The coverslip
274 was returned to the well of the 24 well plate, cells facing up, and wells were washed with
275 PBS (3 x 5 min) with agitation. 250 µl secondary antibodies (streptavidin-Cy3 (SA1010,
276 Sigma) 1:1000; AlexaFluor™ 488 goat anti-rabbit (A11008, Sigma) 1:250) and DAPI ((D9542,
277 Sigma) 1:1000) were added, diluted in 250 µl PBS BSA 1%. Wells were washed with PBS (4 x
278 5 min). From now on, all steps were done protected from light. To anchor the proteins to the
279 gel, we prepared a solution of 5 mg AcX (Acryloyl-X, SE, 6-((acryloyl)amino)hexanoic Acid,
280 Succinimidyl Ester, A20770, Invitrogen) in 500 µl anhydrous DMSO (D12345, Invitrogen); AcX
281 solution was opened and aliquoted in a desiccated environment at – 20°C. AcX was diluted
282 1:100 in PBS, a drop was placed on a piece of parafilm in a humid chamber, the coverslips
283 were placed top-down into the AcX drop and incubated at room temperature for 16 hours.
284 Coverslips were returned to a well of a 24 well plate, washed twice for 5 minutes with PBS
285 and stored in the fridge until the end of the day.
286
287 Monomer solution was prepared with sodium acrylate 8.6% (w/v) (408220, Sigma), AA 2.5%
288 (w/v), N-N'-methylenebisacrylamide 1.5% (w/v) (M7279, Sigma) and NaCl 11.7% (w/v)
289 (AM9760G, Ambion) in PBS; sodium acrylate stock solution 33% (w/v) was freshly prepared
290 by dissolving 1.9 g sodium acrylate in 5 ml of ddH_2O, 0.2 µm-filtered. For gelation, gelling
291 solution was prepared from 100 µl monomer solution, 1 µl 10% APS and 1 µl 10% TEMED,
292 vortexed and used instantly. 50 µl of gelling solution was placed on a piece of parafilm in a
293 humid chamber; the coverslips were placed on top, cells facing downwards, and incubated

294 at 37°C for one hour. After polymerization, coverslips with the gel attached were transferred
295 to a well of a 6-well plate with 1 ml of digestion solution (0.5% Triton X100, 1 mM EDTA pH 8
296 (AM9260G, Ambion), 50 mM Tris pH 8 (AM9855G, Ambion) and 1 M NaCl (AM9760G,
297 Ambion) freshly supplemented with 10 µl proteinase K (P8107S, New England Biolabs).
298 Plates were stored slightly tilted to ensure the coverslip was completely covered with
299 digestion solution and incubated at room temperature overnight. Next day, gels were either
300 already detached from the coverslip or could be easily detached with a spatula. Gels were
301 transferred to a Petri dish and three rounds of expansion, each with 20 ml ddH_2O for 20
302 minutes, were done. After this, a picture was taken to measure the expansion factor. Gel
303 mounting in the imaging chamber and imaging were done as described for UExM.
304

305 **RESULTS**

306

307 **1. TurboID-fusion proteins can be accurately localised with fluorescent streptavidin by light**
308 **microscopy**

309 To establish a robust imaging system for TurboID fusion proteins by streptavidin, we
310 expressed the *T. brucei* nuclear pore proteins NUP110, NUP76 and NUP96 fused to a
311 TurboID-HA tandem tag in procyclic *Trypanosoma brucei* cells using both N and C-terminal
312 fusion for each respective target protein. The tag is composed of the biotin ligase TurboID
313 (Branon et al., 2018) and the HA peptide tag. Expression was constitutive from the
314 endogenous locus and labelling relied on the biotin substate present in the medium (0.8 µM
315 in SDM79) (Moreira et al., 2023). Biotinylated proteins were purified by streptavidin affinity
316 and analysed by liquid chromatography coupled to tandem mass spectrometry (LC-MSMS),
317 using both, wild type cells and cells expressing TurboID-GFP for background correction
318 (Moreira et al., 2023). For each bait protein, we quantified and visualised the biotinylation of
319 all other nuclear pore proteins and known transport factors in *t*-test difference increments
320 (Figure 1A, Figure S1, Table S2). Additionally, we reanalysed previously published data of C-
321 terminally tagged MEX67 and NUP158 in the same way ((Moreira et al., 2023), Figure 1A,
322 Figure S1, Table S2)). Neither of the bait proteins caused biotinylation of the entire pore
323 complex. Instead, we observed highly specific labelling patterns for each bait. While the
324 central NUP96 biotinylated most nuclear pore proteins with the marked exception of the
325 nuclear basket, NUP158 and NUP76 caused biotinylation of specific sub-complexes of the
326 pore and MEX67 labelled NUPs lining the channel of the pore (Moreira et al., 2023). The
327 data show that the labelling radius of TurboID, under these conditions, is below the size of
328 the nuclear pore and thus well below the resolution of light microscopy.

329

330 Next, we imaged cells expressing nuclear pore proteins fused to the TurboID-HA tandem tag
331 using both cy3-streptavidin and anti-HA in combination with a secondary antibody coupled
332 to the Alexa488 fluorophore (Figure 1B). For *T. brucei* NUP132-TurboID-HA, no obvious
333 differences in resolution were observed between antibody-based and streptavidin-based
334 detection (Figure 1C). Likewise, for human NUP88, expressed as N-terminal TurboID-4HA
335 fusion protein in HeLa cells, grown in DMEM medium (relying on the biotin of the serum
336 supplement with a low nanomolar concentration), the signal of anti-HA and of streptavidin

337 appeared highly similar (Figure 1D). Wild type cells of both Trypanosomes and human
338 showed only a very low streptavidin signal, indicating that the signal from naturally
339 biotinylated proteins is neglectable (Figure S8 in supplementary material). The data
340 demonstrate that imaging of Turbo-ID fusion proteins via streptavidin is a reliable
341 alternative, with a resolution that is indistinguishable from antibody-based
342 immunofluorescence in standard light microscopy, which is in agreement with published
343 data on experimentally determined BioID labelling radii (Branon et al., 2018; Kim et al.,
344 2016). The one exception are very motile proteins that produce a "biotinylation trail" distinct
345 to the steady state localisation; these exceptions, and how they can be exploited to
346 understand protein interactions, are discussed in chapter 4 below.
347
348 **2. TurboID-fusion proteins can be imaged in phase separated/protein-dense regions**
349 We had previously expressed one of the *T. brucei* nuclear mRNA transporters, *Tb*MEX67,
350 fused to TurboID-HA and observed that anti-HA failed to stain MEX67 at the nuclear pores,
351 indicating a possible failure of the antibody to either penetrate phase separated areas or to
352 bind the epitope in this environment (details in introduction, (Moreira et al., 2023), Figure
353 2A).
354 To test this hypothesis, we focussed on two additional *bona fine* phase-separated regions:
355 the nucleolus and starvation stress granules. We expressed a C-terminal TurboID-HA fusion
356 of the trypanosome nucleolar GTP-binding protein NOG1 (Tb927.11.3120) (Billington et al.,
357 2023). The resulting streptavidin signal was exclusively at the nucleolus, which is tractable as
358 distinct compartment within the nucleus lacking DAPI fluorescence (Figure 2B). In contrast,
359 the HA-signal showed no obvious accumulation in the nucleolus and was extremely weak
360 with a patchy distribution throughout the entire cell body, indicating an unspecific
361 background stain (Figure 2B). Thus, just like MEX67, the nucleolar protein NOG1 is
362 detectable by streptavidin, but not by anti-HA immunofluorescence. Next, we starved
363 trypanosome cells that were expressing the established starvation stress granule marker
364 PABP2 (Fritz et al., 2015; Kramer et al., 2013) fused to TurboID-HA and probed the cells with
365 the streptavidin anti-HA combination. Both anti-HA and streptavidin readily detected
366 starvation stress granules (Figure 2C). However, the granules detected by anti-HA were in
367 general less distinct and appeared larger than those detected by streptavidin. Indeed,
368 intensity profiles drawn through Z-stack projections of stress granules were 1.4±0.2 -fold

369 wider for anti-HA detection in comparison to streptavidin detection and the corresponding
370 HA profiles frequently exhibited a double-peak (Figure 2D and E). The data are consistent
371 with anti-HA preferentially staining the periphery of the granules, while streptavidin diffuses
372 into and binds within these dense, phase separated particles. A switch of the two
373 fluorophores (Cy3 and Alexa488) gave identical results, controlling for microscopy artefacts
374 as a reason for the differences (Figure S2). Direct eYFP- fluorescence intensity profiles of
375 granules from cells expressing PABP2-eYFP resembled those of the streptavidin stain, ruling
376 out a preferential granule-peripheral localisation of PABP2 as an explanation (Figure S3).
377 Thus, anti-HA fails to label three distinct phase-separated structures of the trypanosome
378 cell, the nuclear pore channel, the nucleolus and the inside of starvation stress granules,
379 while streptavidin faithfully decorates all these structures.
380 The inability of anti-HA to detect target epitopes within phase-separated areas is not
381 restricted to trypanosomes: When expressing TurboID-4HA fusions of the human FG-repeat
382 nucleoporin NUP54 in HeLa cells, streptavidin detected the proteins at the nuclear pores,
383 while no specific anti-HA signal was observed (Figure 2F).
384 Furthermore, the inability to label phase-separated areas is not restricted to anti-HA but
385 applies to other antibodies. We expressed *T. brucei* MEX67 and NOG1 fused to TurboID-Ty1
386 and failed to label the nuclear pores and the nucleolus with anti-Ty1 (BB2), respectively,
387 while the streptavidin signal displayed the correct localisations (Figure 2G and H). Moreover,
388 MEX67 was undetectable at the nuclear pores by polyclonal antiserum (Figure 2I; (Pozzi et
389 al., 2023)) and an eGFP-fusion of MEX67 could not be detected by fluorophore labelled eGFP
390 nanobodies at the pores either (Figure 2J). The absence of a nanobody signal rules out that
391 its simply the size of IgGs that prevents the staining of Mex67 at the nuclear pores, as
392 nanobodies are smaller than (tetrameric) streptavidin. In contrast, an eGFP fusion of NOG1
393 was detectable by eGFP nanobodies at the nucleolus, albeit weakly (Figure 2J). In
394 conclusion, most but not all antibodies/nanobodies were ineffective in phase separated
395 areas.
396
397 **3. Boosting the signal under low-antigen conditions (expansion microscopy, CLEM)**
398 A potential advantage for imaging TurboID fusion proteins with streptavidin is an increased
399 signal: TurboID is expected to cause multiple lysine-biotinylation of both the bait protein and
400 proteins in close proximity, while antibodies only decorate several (polyclonals) or one

401 specific (monoclonals) epitope of a target protein. Indeed, for many TurboID-HA fusion
402 proteins that we analysed by standard light microscopy, the streptavidin signal appeared
403 significantly stronger and devoid of background stain when comparing to anti-HA. To
404 quantify this observation, we probed cells expressing NUP158-TurboID-HA with
405 combinations of anti-HA/Alexa488 secondary antibody and Streptavidin-Cy3 (Figure 3A) or
406 with Streptavidin-Alexa488 and anti-HA/Alexa594 secondary antibody (Figure 3B). Under
407 both labelling conditions, the streptavidin stain resulted in significantly less non-specific
408 cytoplasmic background signal than anti-HA (Figure 3A-B). Moreover, the maximum
409 Alexa488 signal of Z-stack projections was 2.9-fold higher for streptavidin than for anti-HA
410 (N=60, unpaired two-tailed *t*-test=9.6E-55) (Figure 3C). An increase in fluorescence signal is
411 desirable for the detection of low abundance proteins, but also for imaging applications that
412 necessitate a reduction in antigen density, such as expansion microscopy or CLEM.
413
414 In expansion microscopy, biomolecules are covalently cross-linked to a hydrogel, that is
415 subsequently swollen by osmosis, causing a physical magnification of the sample (Chen et
416 al., 2015). Even a relatively small expansion factor of 3 causes a 27-fold increase in sample
417 volume and thus a 27-fold decrease in antigen-density. The two main expansion microscopy
418 methods are Protein-retention Expansion Microscopy (proExM) (Tillberg et al., 2016) and
419 Ultra-structural Expansion Microscopy (U-ExM) (Gambarotto et al., 2019). The main
420 difference is that in proExM, antibody labelling is applied prior to the expansion process,
421 while in U-ExM it is done afterwards. U-ExM thus generally results in higher resolution, as
422 the linkage-error (difference between position of the fluorophore of the secondary antibody
423 and the position of the target protein) is not expanded. Next to the decrease in antigen-
424 density as a consequence of the expansion, the signal is further compromised by the harsh
425 conditions associated with the method, as for example an incubation step at 95°C in alkaline
426 SDS-containing buffer for 90 min for U-ExM and an over-night proteinase K digestion for
427 ProExM. To assess the potential of streptavidin imaging, we employed both proExM and U-
428 ExM on cell lines expressing TurboID-HA fusions of two trypanosome nuclear-pore localised
429 proteins (NUP76 and MEX67) and compared the signals from streptavidin and anti-HA
430 (Figure 3D). For both proteins, streptavidin caused a strong and uniform stain of all nuclear
431 pores with both expansion microscopy methods. In contrast, anti-HA failed to detect nuclear
432 pores either completely (MEX67) or partially (NUP76) in U-ExM. In proExM, pores could be

433 stained evenly with anti-HA, but the signal was much lower in comparison to streptavidin, in
434 particular for NUP76. To our knowledge, this is the first time that streptavidin imaging of a
435 biotin ligase-fused protein was used in combination with expansion microscopy. In our
436 hands, streptavidin clearly outperformed antibodies in both expansion protocols and with
437 both target proteins that we tested, giving a significantly stronger signal with less
438 background.
439
440 CLEM causes an even larger reduction in accessible antigen than expansion microscopy. Thin
441 slices of a resin-embedded sample are first used for immunofluorescence and imaged by
442 light microscopy, and, in a second step, imaged by electron microscopy. The resin largely
443 prevents antibody penetration and probing is therefore restricted to the small fraction of
444 antigens present at the surface of the resin slice. Trypanosome cells expressing NUP96-
445 TurboID-HA or NUP158-TurboID-HA were embedded in LR-white and slices were probed
446 with streptavidin and anti-HA. For both proteins, the streptavidin signal detected numerous
447 pores for each nucleus, while anti-HA detected between 0 and 2 pores and, in addition,
448 caused considerably higher background signals (Figure 3E and Figure S4 in Supplementary
449 materials). Streptavidin is thus more suitable for CLEM, and an example, targeting NUP158-
450 TurboID-HA with both steps, is shown in Figure 3F.
451
452 In summary, streptavidin detection causes a massive increase in signal that is in particularly
453 beneficial under low-antigen density conditions, and thus offers significant implications in
454 expansion microscopy and CLEM.
455
456 **4. Visualization of protein interactions**
457 We found that in most cases, streptavidin labelling faithfully reflects the steady state
458 localisation of a bait protein, e.g., the localisation resembles those observed with
459 immunofluorescence or direct fluorescence imaging of GFP-fusion proteins. For certain bait
460 proteins, this is not the case, for example, if the bait protein or its interactors have a
461 dynamic localisation to distinct compartments, or if interactions are highly transient. It is
462 thus essential to control streptavidin-based *de novo* localisation data by either antibody
463 labelling (if possible) or by direct fluorescence of fusion-proteins for each new bait protein.
464 However, any additional signal from biotinylated partner proteins at a different location can

465 also be leveraged to gain relevant information on the function and dynamics of the bait
466 protein. Three respective examples are detailed below:
467
468 The first is PABP2, one of two trypanosome poly(A) binding proteins, that has established,
469 unambiguous cytoplasmic localisation, when visualised with either anti-HA or when
470 expressed fused to a fluorescent protein (Figure 4A-B, (Billington et al., 2023; Kramer et al.,
471 2013). However, when PABP2-TurboID-HA expressing cells are probed with streptavidin, a
472 signal at the posterior pole of the cell is observed, in addition to the expected cytoplasmic
473 signal (Figure 4A). Localisation to the posterior pole is an exclusive feature of the
474 trypanosome mRNA decapping enzyme ALPH1 and its four interaction partners: a small
475 proportion of this mRNA decapping complex localises to the posterior pole, in a dynamic
476 manner, while the majority remains cytoplasmic (Kramer, 2017; Kramer et al., 2008; Kramer
477 et al., 2023) (Figure 4B). The streptavidin signal at the posterior pole of the PABP2-TurboID-
478 HA cells thus likely reflects a historic cytoplasmic interaction between PABP2 and the mRNA
479 decapping complex. The existence of this interaction is supported by the identification of all
480 five posterior-pole localised members of the decapping complex by mass spectrometry data
481 from a PABP2 BioID experiment (Moreira et al., 2023). Notably, imaging with streptavidin
482 adds information about protein dynamic interactions, that mass spectrometry data alone
483 cannot uncover. In this case, it shows that the fraction of mRNA decapping proteins at the
484 posterior pole is dynamically exchanged with the fraction in the cytoplasm.
485
486 The second example is MLP2 (also called NUP92), a divergent nucleoporin of Kinetoplastida
487 involved in chromosome distribution during mitosis (Holden et al., 2014; Morelle et al.,
488 2015). MLP2 localisation is cell cycle dependent: while exhibiting a nuclear localisation
489 during interphase, it migrates to the spindle and spindle pole during mitosis (Holden et al.,
490 2014; Morelle et al., 2015) (Figure S5). We expressed MLP2 fused to an N-terminal TurboID-
491 HA tag and examined the streptavidin and HA signal in interphase and mitotic cells (Figure
492 4C). Note that in trypanosomes the kinetoplast (mitochondrial DNA, visible as small dot in
493 DAPI stain) divides prior to the nucleus and numbers and positions of kinetoplasts and nuclei
494 are established markers for cell cycle stages (Sherwin and Gull, 1989). We observed that the
495 streptavidin signal “lagged behind” the anti-HA signal at all cell cycle stages. This is most
496 obvious in anaphase, when anti-HA exclusively stains the spindle pole body, while

497 streptavidin decorates both, the nuclei and the spindle pole body. Thus, for proteins with
498 cell-cycle dependent localisation, streptavidin-labelling provides information on both, the
499 previous localisation(s) of the bait, in addition to its current position.
500
501 The third example are nuclear pore proteins. For all NUPs that we tested, we observed the
502 expected streptavidin signal at the nuclear pores (see below). However, for some NUPs, for
503 example NUP65, we observed additional cytoplasmic streptavidin stain that is absent for
504 others, as for example NUP75 (Figure 4 D-E). There were also differences in the amount of
505 nucleoplasmic biotinylation between NUPs. For example, NUP75 showed more nuclear
506 labelling than NUP65 (Figure 4 D-E). The likeliest explanation is, that some NUPs are
507 contacting and thus proximity-labelling proteins in transit. The streptavidin stain in the
508 nucleoplasm or cytoplasm thus provides information about the functions of the individual
509 NUPs in protein import or export, respectively.
510
511 Importantly, tracking of proteins by streptavidin imaging requires orthogonal controls, as the
512 imaging alone does not provide information about the nature of the biotinylated proteins.
513 These can be proximity ligation assay, mass spectrometry or specific tagging visualisation of
514 protein suspects by fluorescent tags. Once these orthogonal controls are established for a
515 specific tracking, streptavidin imaging is an easy and cheap and highly versatile method to
516 monitor protein interactions in a specific setting.
517
518 **5. A phase-separation map of the *T. brucei* nuclear pore**
519 We reasoned that our findings that all phase-separated regions of trypanosomes that we
520 tested are inaccessible to anti-HA can be exploited as a tool for de novo identification of
521 phase-separated regions. As a proof of principle, we employed streptavidin-imaging to
522 produce a map of antibody-inaccessible regions of the entire trypanosome nuclear pore
523 complex. We endogenously expressed all known trypanosome nuclear pore proteins fused
524 to TurboID-HA from one allele. For each protein, two cell lines were constructed, one with
525 TurboID-HA fused to the C-terminus, and one with the tag at the N-terminus. We excluded
526 Mlp2/Nup92, as we found this protein localizing to the nucleus rather than the nuclear
527 pores in most interphase cells (Figure S5 in Supplementary material and Figure 4C), in
528 agreement with (Morelle et al., 2015). For two C-terminal fusion candidate proteins (Sec13,

529 NUP140) and one N-terminal (NUP82), we repeatedly failed to obtain cell lines. The
530 remaining 45 cell lines were controlled by western blot probed with anti-HA to confirm the
531 correct size of the fusion protein (Figure S6). Next, cells from all cell lines were probed with
532 anti-HA and fluorescent streptavidin. All cell lines showed streptavidin signal predominantly
533 at the nuclear pores, proving the correct localisation of the fusion proteins (Figure 5A). For
534 N-terminally tagged NUP64 we also observed between one and two streptavidin dots in the
535 nucleus, consistent with the localisation of eYFP-NUP64 in life cells (Billington et al., 2023); a
536 likely mislocalisation.
537 When evaluating the HA signal at the nuclear pores, we observed no antibody stain for the
538 NUPs lining the central channel, while most NUPs at the periphery of the channel were
539 accessible to the antibody (Figure 5). Importantly, there is no correlation between protein
540 abundancy, as determined by proteomics (Tinti and Ferguson, 2022), and
541 immunofluorescence signal, ruling out low antigen abundance as the reason for its absence
542 (Figure S7). All the FG-NUPs of the inner channel (which are known to phase-separate) were
543 among the non-accessible proteins, supporting the idea that the crucial determinant
544 preventing anti-HA detection is mainly or entirely phase separation. Likewise, the mRNA-
545 interacting NUP76 complex consisting of NUP76 and the FG NUPs NUP140 and NUP149
546 appear non-accessible to anti-HA, except when NUP149 is tagged at the N-terminus. The
547 NUP76 interacting protein NUP158 was inaccessible to antibodies when tagged at the N-
548 terminus, but not at the C-terminus: this is consistent with NUP158 being partially phase-
549 separated as it contains FG-repeats exclusively at the N-terminal half. Among the antibody
550 inaccessible proteins were also some non-FG NUPs. These include proteins of the inner ring,
551 NUP181, NUP144, C-terminally tagged NUP225 and N-terminally tagged NUP65, as well as
552 N-terminally tagged proteins of the outer ring, NUP89 and NUP41. Whether the respective
553 termini of these proteins extend into phase separated areas, or whether antibody access is
554 prevented by steric or other hindrances remains unknown.
555 In conclusion, we here provide an antibody access map of the entire *T. brucei* nuclear pore
556 that includes all bone-fine FG-NUPs in addition to some non-FG NUPs.
557
558
559

560 **DISCUSSION**

561 We here show that the use of the TurboID-HA tandem tag offers an "all in one" solution to
562 antibody-accessibility problems, without compromising resolution or the strength of the
563 signal. Quite the contrary, streptavidin imaging of TurboID-HA tagged proteins facilitates a
564 massive boost in signal, extending the benefits of the method to protein targets with low
565 antigen abundance. Furthermore, the TurboID-HA tag is suitable to probe protein
566 interactions and provide some evidence for phase-separation.

567

568 Like many methods that are frequently used in cell- and molecular biology, streptavidin
569 imaging is based on the expression of a genetically engineered fusion protein: it is essential
570 to validate both, function and localisation of the TurboID-HA tagged protein by orthogonal
571 methods. If the fusion protein is non-functional or mis-localised, tagging at the other end
572 may help, but if not, this protein cannot be imaged by streptavidin imaging. Likewise, target
573 organisms not amenable to genetic manipulation, or those with restricted genetic tools, are
574 not or less suitable for this method.

575

576 **One protocol suits all - streptavidin readily traces biotin proximity labels**

577 Many proteins are not accessible to antibodies in standard immunofluorescence protocols,
578 in particular proteins localized in phase-separated regions. MEX67 could not be detected at
579 the trypanosome nuclear pore by anti-HA, anti-Ty1, anti-Protein A, polyclonal MEX67
580 antibodies and even nanobodies to mNeonGreen (this work, (Dostalova et al., 2013; Moreira
581 et al., 2023; Pozzi et al., 2023)); likewise, the human Mex67 homologue TAP/Nxf1 evaded
582 detection by antiserum (Bear et al., 1999). HA-fused trypanosome FG-NUPs and the human
583 FG-NUP NUP54 could not be decorated with anti-HA. Trypanosome starvation stress
584 granules could only be labelled at the periphery and nucleolar proteins evaded antibody
585 detection in trypanosomes (Figure 2) and in human cells (Misteli, 2008; Musinova et al.,
586 2011; Sheval et al., 2005; Zatsepina et al., 1997). There are several approaches available to
587 trouble-shoot antigen-accessibility problems (Piña et al., 2022). Pre-extraction steps prior to
588 fixation employing Triton X100, high salt or nucleases proved successful for the detection of
589 mammalian Mex67 homologue TAP/NXF1 (Ben-Yishay et al., 2019; Katahira et al., 1999).
590 Antibody penetration to nucleolar proteins was improved by including protease treatment
591 (Svistunova et al., 2011). Further, fixation by cold methanol instead of paraformaldehyde

592 was reported to increase antibody access to proteins (Neuhaus et al., 1998). However, the
593 search for individual solutions for each problematic antibody/antigen pair is cumbersome
594 and an improvement of antibody access typically comes at the expense of signal loss and/or
595 disruption of cellular morphology (Piña et al., 2022). With streptavidin labelling we present a
596 method that works for every protein (we tested ~30), without compromising cellular
597 morphology and, most importantly, provides a strong signal as significant additional benefit.
598
599 In standard light microscopy, streptavidin imaging offers a resolution comparable to labelling
600 with antibodies. The labelling radius of the biotin ligase BirA was estimated to be
601 approximately 10 nm by using the NUP107-160 Y-complex of the mammalian nuclear pore
602 as a molecular ruler (Kim et al., 2014), enabling for example the determination of
603 substructures of P-bodies and stress granules (Youn et al., 2018). It is thus within the range
604 of an average-sized protein and well below the resolution limit of light microscopy.
605 Consistently, cells expressing nuclear membrane associated proteins fused to BirA (or
606 variants as the related BioID2) can be probed by fluorescent streptavidin with resolutions
607 that are undistinguishable from probing with the respective IgG antibodies (Kim et al., 2016;
608 May et al., 2020). For the biotin ligase variant TurboID, which has a massively decreased
609 labelling time, the biotin labelling radius was measured to be in a similar (Branon et al.,
610 2018; Kim et al., 2016) or slightly larger range (May et al., 2020). Importantly, the addition of
611 50 µM external biotin massively increased the labelling radius, while in the absence of
612 excessive biotin, the labelling radius remained comparable to the labelling radius of BirA
613 (May et al., 2020). In this work, we avoided the addition of additional biotin to the
614 trypanosome medium (the medium contains 0.8 µM biotin) and serum biotin
615 (approximately 2 nM in mammalian serum (Luong and Vashist, 2020)) was the sole source in
616 HeLa cell medium. Our mass spectrometry data of streptavidin-affinity purified proteins with
617 five nuclear pore localised TurboID-fusion proteins demonstrates that the labelling radius is
618 well below the size of the nuclear pore complex under these conditions, and thus in
619 agreement with published data. Even in expansion microscopy, with 3.6 to 4.2 -fold
620 expansion factors, we did not notice any decrease in resolution; in fact, we could resolve
621 NUPs that reside at different positions within the pore (e.g. inner ring vs basket) by labelling
622 one with streptavidin and the other with an antibody and thus obtained sub-NUP imaging
623 resolution (our own unpublished data). Even though, theoretically, BioID *per se* causes a

624 decrease in resolution as biotinylation extends to proteins in close proximity to the bait, this
625 may well be compensated by the lower linkage error when imaging directly via the small,
626 compact-shaped streptavidin-tetramer rather than by a tandem assembly of two large IgG
627 antibodies (Figure 1B).
628
629 **Streptavidin tracing of biotin proximity labels delivers high signal intensities.**
630 One major benefit of streptavidin imaging was the increase in signal compared to
631 immunofluorescence, caused by multiple biotinylation sites of the bait and adjacent proteins
632 serving as an enhancer. An increased signal is beneficial for almost all protein-imaging
633 applications, but in particular for low abundance targets. Most strikingly, streptavidin
634 imaging facilitates imaging targets with low densities as a consequence of the imaging
635 method, as in expansion microscopy and CLEM and is applicable to all target proteins that
636 tolerate tag fusion to either terminus. Fluorescent streptavidin has been previously used in
637 expansion microscopy to detect biotin residues in target proteins produced by click
638 chemistry (Sun et al., 2021). However, to the best of our knowledge, this is the first report
639 that employs fluorescent streptavidin as a signal enhancer in expansion microscopy and
640 CLEM, by combining it with multiple biotinylation sites added by a biotin ligase. Importantly,
641 for both CLEM and expansion, streptavidin imaging is the only alternative approach to
642 immunofluorescence, as denaturing conditions associated with these methods rule out
643 direct imaging of fluorescent tags.
644
645 **A combination tag as probe for phase separated areas.**
646 A further important application of the TurboID-HA tandem tag is the *de novo* prediction of
647 phase separated areas in cells. The importance of compartmentalization by liquid-liquid
648 phase separation for almost all cellular functions, including DNA and mRNA metabolism (Dai
649 and Yang, 2023), cell division (Ong and Torres, 2020) and development (So et al., 2021)
650 becomes increasingly evident. Aberrant phase separation can cause disease, as for example
651 neurodegenerative disorders (Chakraborty and Zweckstetter, 2023; Tsoi et al., 2023),
652 underlining the relevance of novel tools for identification and characterization of phase
653 separated regions. For individual proteins, phase separation can be predicted in silico using
654 machine learning, with limited, but increasing accuracy (Venko and Žerovnik, 2023). For a
655 defined mixture of molecules, phase separation can be tested in vitro (Alberti et al., 2018;

656 Zhang and Shen, 2023). However, methods to test phase separation in the cellular context
657 are scarce. The correlation between antibody-inaccessibility and phase separation, that we
658 observed in this study, offers the opportunity to use the TurboID-HA tag to probe for phase
659 separation *de novo*. Notably, the streptavidin stain concomitantly provides a convenient
660 intrinsic control to confirm correct localization of the fusion protein. Moreover, proteins with
661 complex localization patterns can be simultaneously detected in both, phase-separated and
662 non-phase separated regions, as we demonstrated for tracing MEX67 to both, the
663 nucleoplasm and nuclear pores (Figure 1A and G). In trypanosomes, all *bonafide* phase-
664 separated regions were inaccessible to anti-HA, namely the nucleolus, starvation stress
665 granules and the FG NUP environment. The data strongly suggest that the absence of an HA
666 immunofluorescence signal correlates with phase-separation. However, we cannot rule out
667 the possibility, that some proteins may be inaccessible to anti-HA for different reasons, as for
668 example steric hindrance. The latter scenario would equally favor streptavidin over IgG
669 antibodies for target protein binding due to its much smaller dimensions and higher binding
670 affinity. We observed some non-FG Nups to be anti-HA inaccessible, which were mostly
671 NUPs of the inner ring, close to the core of FG NUPs: whether these NUPs localize to phase-
672 separated areas is not known. Importantly, problems to detect phase-separated proteins by
673 antibodies appear conserved across species (Bear et al., 1999; Misteli, 2008; Musinova et al.,
674 2011; Sheval et al., 2005; Zatsepina et al., 1997). We show data for the human FG-NUP
675 Nup54 as an example of an anti-HA-inaccessible protein (Figure 2F) as proof of principle,
676 that the *de novo* identification of phase-separation is applicable to human cells.
677 Why are most antibodies and, to some extent even fluorophore conjugated nanobodies,
678 prevented from labelling proteins in phase separated environments, while streptavidin never
679 fails? We cannot distinguish whether the lack in labelling is caused by an access problem of
680 the antibody penetrating the phase separated area or by a reduced binding affinity between
681 antibody and antigen in phase-separated environments, or by a combination of both. Still,
682 the smaller size of streptavidin in comparison to an IgG tandem-antibody pair (Figure 1b)
683 likely favors its access into dense regions. Further, IgG antibodies as well as single chain
684 antibodies typically have affinities in the nanomolar range, comparing to femtomolar affinity
685 of the biotin-streptavidin interaction, which is indeed among the strongest non-covalent
686 interactions in nature (Chivers et al., 2011). Together with the extremely high structural
687 stability of streptavidin towards temperature, pH and denaturing conditions (Laitinen et al.,

688 2006) this can explain the ability of this probe to potently outperform antibodies in phase
689 separated environments.
690
691 **Proximity-labelling reports a history of dynamic protein interactions**
692 Lastly, we propose streptavidin imaging as a novel tool to monitor dynamic interactions
693 between proteins. Since BioID proximity labeling is not restricted to the bait protein, but
694 extends to all interacting partners, the history of interactions is preserved. Hence, changes in
695 protein sub-complexes can be imaged over time. We provide three examples, covering
696 protein complex dynamics in cell cycle regulation and mRNA metabolism as well as nuclear
697 transport. There are many other potential applications. While we relied on an endogenous,
698 constitutive expression of TurboID fusion proteins, a tightly controlled, inducible system, as
699 for example Split-TurboID (Cho et al., 2020) in combination with light activation (Chen et al.,
700 2022; Shafraz et al., 2023) would allow pulse chase experiment, delivering quantitative data
701 on the kinetics of processes.
702
703
704
705 Altogether, streptavidin imaging is a highly versatile tool with multiple applications, ranging
706 from a simple boost in signal that can be leveraged to increase imaging sensitivity in
707 expansion microscopy and CLEM, to the ability to probe for phase-separated areas and to
708 monitor dynamic protein interactions. It is thus an important addition to the available
709 imaging toolbox.
710
711
712 **ACKNOWLEDGEMENT**
713 The work was financed by a bilateral GACR/DFG grant (project IDs.: 21-19503J and
714 KR4017/9-1; to M. Z. and S. K., respectively). We are grateful to the OMICS Proteomics
715 BIOCEV core facility for excellent technical service. We thank Mark Carrington (University of
716 Cambridge, UK) for providing anti-TbMEX67. Manfred Alsheimer is acknowledged for
717 providing advice and plasmids on HeLa cell transfections, Christian Janzen for the BB2
718 antibody and Elisabeth Meyer-Natus and Tim Krüger for help with microscopy and image
719 analysis (all University of Würzburg, Germany).

720

721

722 **FIGURE LEGENDS**

723

724 **Figure 1: The TurboID biotinylation labelling radius is sufficiently small to allow**
725 **streptavidin-based imaging of target proteins by light microscopy**

726 **A)** Schematic representation of the trypanosome NPC (Obado et al., 2016) including selected
727 transport factors and their enrichment observed in TurboID experiments followed by
728 streptavidin affinity capture and LC MS/MS analysis. Proteins quantified are filled in shades
729 of green representative of the corresponding *t*-test difference increments. The respective
730 bait protein is drawn in pink and undetected proteins are in gray. NUP96, NUP76 and
731 NUP110 experiments were analysed with TurboID-HA fusions at both respective termini (as
732 indicated). The nuclear envelope is drawn in sand and nucleoporins and transport factors are
733 numbered in the legend (right) according to (Obado et al., 2016) (NMD3, Tb927.7.970;
734 RanBP1, Tb927.11.3380; RanBPL, Tb927.10.8650; exportin 1, Tb927.11.14340; GAP,
735 Tb927.10.7680),

736 **B)** Schematics illustrating the imaging concept for a protein of interest (POI) by either Cy3-
737 streptavidin or anti-HA coupled with secondary Alexa488-labelled antibodies.

738 **(C-D)** Nuclear pore proteins of *Trypanosoma brucei* (C) and HeLa cells (D) were expressed
739 fused to the streptavidin-HA tandem tag and detected with streptavidin-cy3 (pink) and anti-
740 HA (green). Representative single plane images of a Z-stack is shown, as raw data.

741

742 **Figure 2: Streptavidin can detect targets within phase-separated regions, while most**
743 **antibodies fail**

744 **(A-B)** *T. brucei* MEX67 (A) and *T. brucei* nucleolar protein NOG1 (B) were expressed fused to a
745 C-terminal TurboID-HA tandem tag and cells probed with streptavidin-cy3 (pink) and by anti-
746 HA immunofluorescence (green). Representative single plane images of an unprocessed Z-
747 stack series are shown.

748 **(C-E)** Cells expressing the stress granule marker protein PABP2 fused to TurboID-HA were
749 starved (2 hours PBS) and starvation stress granules detected by streptavidin (pink, Cy3) and
750 anti-HA (green, Alexa488). The starvation experiment was performed in biological triplicates.
751 One representative image of starved cells is shown as Z-stack projection (72 slices a 140 nm,
752 sum slices) in C. For each replicate, intensity profiles across one of the larger granules of the
753 cell were measured for 25 cells in both fluorescence channels. The profiles for replicate 1 are

754 shown in D. For each granule, the granule diameter was calculated from the profiles at 50%
755 fluorescence and the difference in diameter between the HA- and streptavidin stain is
756 presented in E for each replicate, as quotient of granule diameters. Note that despite
757 differences between the three replicates, likely arisen from starvation conditions being not
758 100% reproducible, the HA stain consistently delivered a larger granule diameter than the
759 streptavidin stain, consistent with preferentially peripheral staining of the granule by anti-
760 HA. For replicate 2, the fluorophores were switched, with essentially the same result (Figure
761 S2 in Supplementary Materials).
762 **(F)** Human NUP54 fused to TurboID-4HA was expressed in HeLa cells and cells were probed
763 with both anti-HA (green, Alexa488) and streptavidin (Cy3, shown in pink). Streptavidin, but
764 not anti-HA detects NUP54 at the nuclear pores. A single plane image of a Z-stack is shown
765 as raw data.
766 **(G and H)** *T. brucei* MEX67 (G) and NOG1 (H) were expressed as TurboID-Ty1 fusion proteins
767 and detected with streptavidin (Cy3, shown in pink) and anti-Ty1 (BB2, green).
768 Representative single plane images of unprocessed Z-stack images are shown.
769 **(I)** Trypanosome wild type (WT) cells were probed for MEX67 with polyclonal antiserum
770 (kind gift of Mark Carrington, University of Cambridge; secondary antibody Alexa 488, shown
771 in pink). One representative single plane image of an unprocessed Z-stack image is shown.
772 **(J)** *T. brucei* MEX67 (left) and NOG1 (right) were expressed as eGFP fusion proteins and
773 detected with Cy5 labelled eGFP nanobodies. Representative single plane images of
774 unprocessed Z-stack images are shown.
775
776 **Figure 3: Streptavidin imaging yields higher signal intensities than immunofluorescence**
777 **(A-C) Enhanced signal in standard light microscopy**
778 Trypanosome cells expressing NUP158-TurboID-HA were labelled with combinations of
779 either streptavidin-Cy3 and anti-HA/Alexa488 secondary (A) or with streptavidin-Alexa488
780 and anti-HA//Alexa 594 secondary (B). Z-stack images were recorded (48 slices a 140 nm).
781 Representative, unprocessed single plane images are shown (A and B). The maximum
782 Alexa488 fluorescence was quantified from Z-stack projections (sum slices) from 60 cells
783 probed with anti-HA or streptavidin; the data are presented as a dot blot (waist is median;
784 box is IQR; whiskers are ± 1.5 IQR) (C)
785 **(D) Improved signal in expansion microscopy**

786 Trypanosome cells expressing NUP76-TurboID-HA or MEX67-TurboID-HA were imaged using
787 Pro-expansion or Ultra-expansion microscopy. Single plane and Z-stack projections (sum
788 slices) of the streptavidin and anti-HA signal are shown for one representative nucleus. All
789 images were deconvolved in proExM, except for NUP76 $_{anti}$-HA.
790 **(E-F) Improved signal in CLEM**
791 Trypanosome cells expressing NUP158-TurboID-HA were embedded in LR-White resin. Slices
792 were probed with streptavidin and anti-HA and imaged by light microscopy (E) followed by
793 electron microscopy (CLEM) (F).
794
795 **Figure 4: Visualisation of protein interactions with TurboID**
796 **(A)** Trypanosome cells expressing PABP2-TurboID-HA were probed with streptavidin and
797 anti-HA. A representative image of the posterior part of a cell is shown (single plane of a Z-
798 stack processed by computational clearing). The position of posterior pole granule is
799 indicated by arrows.
800 **(B)** Trypanosome cells were transformed to co-express PABP2-mChFP and ALPH1-eYFP. A
801 representative image of the posterior part of a cell is shown (single plane of a Z-stack
802 processed by deconvolution). The position of posterior pole granule is indicated by arrows.
803 **(C)** Trypanosome cells expressing TurboID-HA-MLP2 were probed with streptavidin and anti-
804 HA. One representative image of an interphase, prophase, metaphase and an anaphase cell
805 are shown. All images are unprocessed single plane images, with the exception of the DAPI
806 image that is a Z-stack projection (max intensity of 48 slices a 140 nm).
807 **(D and E)** Trypanosome cells expressing NUP65 (D) or NUP75 (E) fused to a C-terminal
808 TurboID-HA tag were probed with streptavidin. Single plane and Z-stack projection (sum
809 slices of 48 slices a 140 m) of unprocessed images are shown.
810
811 **Figure 5: A refined map of the *T. brucei* nuclear pore complex**
812 Each known *T. brucei* nuclear pore protein was expressed fused to TurboID-HA, each both at
813 the N- and C-terminus. Cells were labelled with anti-HA and with streptavidin.
814 **(A)** For each NUP, a representative image of the nucleus is shown as unprocessed, single
815 plane of a Z-stack. We evaluated the extent of anti-HA stain in colour increments (shown as a
816 bar above images).

817 **(B)** The HA-signal at the nuclear pores was mapped onto a schematic representation of the
818 trypanosome NPC (modified from (Obado et al., 2016)) using the same colour increments.
819 **(C)** Scheme of the *T. brucei* nuclear pore, with known FG NUPs (Obado et al., 2016) shown in
820 black on the left side and prediction of phase separation (Chu et al., 2022) mapped on the
821 right.
822
823 Figure S1: Statistical analysis of NUP TurboID experiments
824 Figure S2: colour Swap PABP2-TurboID-HA
825 Figure S3: PABP2-eYFP starved and profile
826 Figure S4: LR White probing NUP158, NUP96
827 Figure S5: Mlp2/Nup92, image with many cells, both C and N terminal
828 Figure S6: Western blots Phase ID
829 Figure S7: no correlation between antigen abundance and absence of HA signal
830 Figure S8: streptavidin signal from wild type cells is neglectable
831 Table S1: List of all plasmids used in this work.
832 Table S2: NUP TurboID proteomics data and statistical analysis.
833
834

835 **LITERATURE**

836
837

838 **Alberti, S., Saha, S., Woodruff, J. B., Franzmann, T. M., Wang, J. and Hyman, A. A.** (2018). A
839 User's Guide for Phase Separation Assays with Purified Proteins. *Journal of Molecular*
840 *Biology* 1–15.

841 **Aslett, M., Aurrecoechea, C., Berriman, M., Brestelli, J., Brunk, B. P., Carrington, M.,**
842 **Depledge, D. P., Fischer, S., Gajria, B., Gao, X., et al.** (2010). TriTrypDB: a functional
843 genomic resource for the Trypanosomatidae. *Nucleic Acids Research* **38**, D457-62.

844 **Bear, J., Tan, W., Zolotukhin, A. S., Tabernero, C., Hudson, E. A. and Felber, B. K.** (1999).
845 Identification of Novel Import and Export Signals of Human TAP, the Protein That Binds
846 to the Constitutive Transport Element of the Type D Retrovirus mRNAs. *Mol. Cell. Biol.*
847 **19**, 6306–6317.

848 **Ben-Yishay, R., Mor, A., Shraga, A., Ashkenazy-Titelman, A., Kinor, N., Schwed-Gross, A.,**
849 **Jacob, A., Kozer, N., Kumar, P., Garini, Y., et al.** (2019). Imaging within single NPCs
850 reveals NXF1's role in mRNA export on the cytoplasmic side of the pore. *J. Cell Biol.* **218**,
851 2962–2981.

852 **Billington, K., Halliday, C., Madden, R., Dyer, P., Barker, A. R., Moreira-Leite, F. F.,**
853 **Carrington, M., Vaughan, S., Hertz-Fowler, C., Dean, S., et al.** (2023). Genome-wide
854 subcellular protein map for the flagellate parasite Trypanosoma brucei. *Nat. Microbiol.* **8**,
855 533–547.

856 **Branon, T. C., Bosch, J. A., Sanchez, A. D., Udeshi, N. D., Svinkina, T., Carr, S. A., Feldman, J.**
857 **L., Perrimon, N. and Ting, A. Y.** (2018). Efficient proximity labeling in living cells and
858 organisms with TurboID. *Nature biotechnology* **36**, 880–887.

859 **Brun, R. and Schönenberger** (1979). Cultivation and in vitro cloning or procyclic culture
860 forms of Trypanosoma brucei in a semi-defined medium. Short communication. *Acta*
861 *tropica* **36**, 289–292.

862 **Chakraborty, P. and Zweckstetter, M.** (2023). Role of aberrant phase separation in
863 pathological protein aggregation. *Curr. Opin. Struct. Biol.* **82**, 102678.

864 **Chen, F., Tillberg, P. W. and Boyden, E. S.** (2015). Expansion microscopy. *Science* **347**, 543–
865 548.

866 **Chen, R., Zhang, N., Zhou, Y. and Jing, J.** (2022). Optical Sensors and Actuators for Probing
867 Proximity-Dependent Biotinylation in Living Cells. *Front Cell Neurosci* **16**, 801644.

868 **Chivers, C. E., Koner, A. L., Lowe, E. D. and Howarth, M.** (2011). How the biotin–
869 streptavidin interaction was made even stronger: investigation via crystallography and a
870 chimaeric tetramer. *Biochem. J.* **435**, 55–63.

871 **Cho, K. F., Branon, T. C., Rajeev, S., Svinkina, T., Udeshi, N. D., Thoudam, T., Kwak, C.,**
872 **Rhee, H.-W., Lee, I.-K., Carr, S. A., et al.** (2020). Split-TurboID enables contact-dependent
873 proximity labeling in cells. *Proc National Acad Sci* **117**, 12143–12154.

874 **Chu, X., Sun, T., Li, Q., Xu, Y., Zhang, Z., Lai, L. and Pei, J.** (2022). Prediction of liquid–liquid
875 phase separating proteins using machine learning. *BMC Bioinform.* **23**, 72.

876 **Cox, J. and Mann, M.** (2008). MaxQuant enables high peptide identification rates,
877 individualized p.p.b.-range mass accuracies and proteome-wide protein quantification.
878 *Nature biotechnology* **26**, 1367–1372.

879 **Cox, J., Hein, M. Y., Luber, C. A., Paron, I., Nagaraj, N. and Mann, M.** (2014). Accurate
880 Proteome-wide Label-free Quantification by Delayed Normalization and Maximal Peptide
881 Ratio Extraction, Termed MaxLFQ*. *Mol Cell Proteomics* **13**, 2513–2526.

882 **Dai, Z. and Yang, X.** (2023). The regulation of liquid-liquid phase separated condensates
883 containing nucleic acids. *FEBS J.*

884 **Davis, L. K., Ford, I. J. and Hoogenboom, B. W.** (2022). Crowding-induced phase separation
885 of nuclear transport receptors in FG nucleoporin assemblies. *eLife* **11**, e72627.

886 **Dean, S., Sunter, J., Wheeler, R. J., Hodkinson, I., Gluenz, E. and Gull, K.** (2015). A toolkit
887 enabling efficient, scalable and reproducible gene tagging in trypanosomatids. *Open*
888 *biology* **5**, 140197.

889 **Derrer, C. P., Mancini, R., Vallotton, P., Huet, S., Weis, K. and Dultz, E.** (2019). The RNA
890 export factor Mex67 functions as a mobile nucleoporin. *The Journal of Cell Biology* **218**,
891 3967–3976.

892 **Dostalova, A., Käser, S., Cristodero, M. and Schimanski, B.** (2013). The nuclear mRNA
893 export receptor Mex67-Mtr2 of Trypanosoma brucei contains a unique and essential zinc
894 finger motif. *Molecular Microbiology* **88**, 728–739.

895 **Fritz, M., Vanselow, J., Sauer, N., Lamer, S., Goos, C., Siegel, T. N., Subota, I., Schlosser, A.,**
896 **Carrington, M. and Kramer, S.** (2015). Novel insights into RNP granules by employing the
897 trypanosome's microtubule skeleton as a molecular sieve. *Nucleic Acids Research* **43**,
898 8013–8032.

899 **Gambarotto, D., Zwettler, F. U., Guennec, M. L., Schmidt-Cernohorska, M., Fortun, D.,**
900 **Borgers, S., Heine, J., Schloetel, J. G., Reuss, M., Unser, M., et al.** (2019). Imaging cellular
901 ultrastructures using expansion microscopy (U-ExM). *Nat Methods* **16**, 71–74.

902 **Gambarotto, D., Hamel, V. and Guichard, P.** (2020). Ultrastructure expansion microscopy
903 (U-ExM). *Methods Cell Biol* **161**, 57–81.

904 **Holden, J. M., Koreny, L., Obado, S., Ratushny, A. V., Chen, W. M., Chiang, J. H., Kelly, S.,**
905 **Chait, B. T., Aitchison, J. D., Rout, M. P., et al.** (2014). Nuclear pore complex evolution: a

906 trypanosome Mlp analogue functions in chromosomal segregation but lacks
907 transcriptional barrier activity. *Molecular biology of the cell* **25**, 1421–1436.

908 **Katahira, J., Strässer, K., Podtelejnikov, A., Mann, M., Jung, J. U. and Hurt, E.** (1999). The
909 Mex67p-mediated nuclear mRNA export pathway is conserved from yeast to human. *The*
910 *EMBO journal* **18**, 2593–2609.

911 **Kelly, S., Reed, J., Kramer, S., Ellis, L., Webb, H., Sunter, J., Salje, J., Marinsek, N., Gull, K.,**
912 **Wickstead, B., et al.** (2007). Functional genomics in Trypanosoma brucei: a collection of
913 vectors for the expression of tagged proteins from endogenous and ectopic gene loci.
914 *Molecular & Biochemical Parasitology* **154**, 103–109.

915 **Kim, D. I., Birendra, K. C., Zhu, W., Motamedchaboki, K., Doye, V. and Roux, K. J.** (2014).
916 Probing nuclear pore complex architecture with proximity-dependent biotinylation.
917 *Proceedings of the National Academy of Sciences of the United States of America* **111**,
918 E2453-61.

919 **Kim, D. I., Jensen, S. C., Noble, K. A., KC, B., Roux, K. H., Motamedchaboki, K. and Roux, K.**
920 **J.** (2016). An improved smaller biotin ligase for BioID proximity labeling. *Mol. Biology Cell*
921 **27**, 1188–1196.

922 **Köhler, A. and Hurt, E.** (2007). Exporting RNA from the nucleus to the cytoplasm. *Nature*
923 *Reviews Molecular Cell Biology* **8**, 761–773.

924 **Kramer, S.** (2017). The ApaH-like phosphatase TbALPH1 is the major mRNA decapping
925 enzyme of trypanosomes. *PLoS Pathogens* **13**, e1006456.

926 **Kramer, S., Queiroz, R., Ellis, L., Webb, H., Hoheisel, J. D., Clayton, C. E. and Carrington, M.**
927 (2008). Heat shock causes a decrease in polysomes and the appearance of stress granules
928 in trypanosomes independently of eIF2(alpha) phosphorylation at Thr169. *Journal of Cell*
929 *Science* **121**, 3002–3014.

930 **Kramer, S., Kimblin, N. C. and Carrington, M.** (2010). Genome-wide in silico screen for
931 CCCH-type zinc finger proteins of Trypanosoma brucei, Trypanosoma cruzi and
932 Leishmania major. *BMC genomics* **11**, 283.

933 **Kramer, S., Bannerman-Chukualim, B., Ellis, L., Boulden, E. A., Kelly, S., Field, M. C. and**
934 **Carrington, M.** (2013). Differential Localization of the Two T. brucei Poly(A) Binding
935 Proteins to the Nucleus and RNP Granules Suggests Binding to Distinct mRNA Pools. *PLoS*
936 *ONE* **8**, e54004.

937 **Kramer, S., Meyer-Natus, E., Stigloher, C., Thoma, H., Schnaufer, A. and Engstler, M.**
938 (2020). Parallel monitoring of RNA abundance, localization and compactness with
939 correlative single molecule FISH on LR White embedded samples. *Nucleic Acids Res* **49**,
940 gkaa1142-.

941 **Kramer, S., Karolak, N. K., Odenwald, J., Gabiatti, B., Londoño, P. A. C., Zavřelová, A.,**
942 **Freire, E. R., Almeida, K. S., Braune, S., Moreira, C., et al.** (2023). A unique mRNA
943 decapping complex in trypanosomes. *Nucleic Acids Res.* **51**, 7520–7540.

944 **Laitinen, O. H., Hytönen, V. P., Nordlund, H. R. and Kulomaa, M. S.** (2006). Genetically
945 engineered avidins and streptavidins. *Cell. Mol. Life Sci. CMLS* **63**, 2992–3017.

946 **Luong, J. H. T. and Vashist, S. K.** (2020). Chemistry of Biotin–Streptavidin and the Growing
947 Concern of an Emerging Biotin Interference in Clinical Immunoassays. *ACS Omega* **5**, 10–
948 18.

949 **Mangus, D. A., Evans, M. C. and Jacobson, A.** (2003). Poly(A)-binding proteins:
950 multifunctional scaffolds for the post-transcriptional control of gene expression. *Genome*
951 *biology* **4**, 223.

952 **May, D. G., Scott, K. L., Campos, A. R. and Roux, K. J.** (2020). Comparative Application of
953 BioID and TurboID for Protein-Proximity Biotinylation. *Cells* **9**, 1070.

954 **McCulloch, R., Vassella, E., Burton, P., Boshart, M. and Barry, J. D.** (2004). Transformation
955 of monomorphic and pleomorphic Trypanosoma brucei. *Methods in molecular biology*
956 *(Clifton, NJ)* **262**, 53–86.

957 **Misteli, T.** (2008). Physiological importance of RNA and protein mobility in the cell nucleus.
958 *Histochem. Cell Biol.* **129**, 5–11.

959 **Moreira, C. M. do N., Kelemen, C. D., Obado, S. O., Zahedifard, F., Zhang, N., Holetz, F. B.,**
960 **Gauglitz, L., Dallagiovanna, B., Field, M. C., Kramer, S., et al.** (2023). Impact of inherent
961 biases built into proteomic techniques: Proximity labeling and affinity capture compared.
962 *J Biol Chem* **299**, 102726.

963 **Morelle, C., Sterkers, Y., Crobu, L., MBang-Benet, D. E., Kuk, N., Portalès, P., Bastien, P.,**
964 **Pagès, M. and Lachaud, L.** (2015). The nucleoporin Mlp2 is involved in chromosomal
965 distribution during mitosis in trypanosomatids. *Nucleic Acids Research* **43**, 4013–4027.

966 **Musinova, Y. R., Lisitsyna, O. M., Golyshev, S. A., Tuzhikov, A. I., Polyakov, V. Y. and**
967 **Sheval, E. V.** (2011). Nucleolar localization/retention signal is responsible for transient
968 accumulation of histone H2B in the nucleolus through electrostatic interactions. *Biochim.*
969 *Biophys. Acta (BBA) - Mol. Cell Res.* **1813**, 27–38.

970 **Nag, N., Sasidharan, S., Uversky, V. N., Saudagar, P. and Tripathi, T.** (2022). Phase
971 separation of FG-nucleoporins in nuclear pore complexes. *Biochimica Et Biophysica Acta*
972 *Bba - Mol Cell Res* **1869**, 119205.

973 **Neuhaus, E. M., Horstmann, H., Almers, W., Maniak, M. and Soldati, T.** (1998). Ethane-
974 Freezing/Methanol-Fixation of Cell Monolayers: A Procedure for Improved Preservation
975 of Structure and Antigenicity for Light and Electron Microscopies. *J. Struct. Biol.* **121**,
976 326–342.

977 **Obado, S. O., Brillantes, M., Uryu, K., Zhang, W., Ketaren, N. E., Chait, B. T., Field, M. C.**
978 **and Rout, M. P.** (2016). Interactome Mapping Reveals the Evolutionary History of the
979 Nuclear Pore Complex. *PLoS biology* **14**, e1002365.

980 **Ong, J. Y. and Torres, J. Z.** (2020). Phase Separation in Cell Division. *Mol Cell* **80**, 9–20.

981 **Perez-Riverol, Y., Csordas, A., Bai, J., Bernal-Llinares, M., Hewapathirana, S., Kundu, D. J.,**
982 **Inuganti, A., Griss, J., Mayer, G., Eisenacher, M., et al.** (2019). The PRIDE database and
983 related tools and resources in 2019: improving support for quantification data. *Nucleic*
984 *Acids Research* **47**, D442–D450.

985 **Piña, R., Santos-Díaz, A. I., Orta-Salazar, E., Aguilar-Vazquez, A. R., Mantellero, C. A.,**
986 **Acosta-Galeana, I., Estrada-Mondragon, A., Prior-Gonzalez, M., Martinez-Cruz, J. I. and**
987 **Rosas-Arellano, A.** (2022). Ten Approaches That Improve Immunostaining: A Review of
988 the Latest Advances for the Optimization of Immunofluorescence. *Int. J. Mol. Sci.* **23**,
989 1426.

990 **Pozzi, B., Naguleswaran, A., Florini, F., Rezaei, Z. and Roditi, I.** (2023). The RNA export
991 factor TbMex67 connects transcription and RNA export in Trypanosoma brucei and sets
992 boundaries for RNA polymerase I. *Nucleic Acids Res.* **51**, 5177–5192.

993 **Rappsilber, J., Mann, M. and Ishihama, Y.** (2007). Protocol for micro-purification,
994 enrichment, pre-fractionation and storage of peptides for proteomics using StageTips.
995 *Nat Protoc* **2**, 1896–1906.

996 **Rodriguez, M. S., Dargemont, C. and Stutz, F.** (2004). Nuclear export of RNA. *Biol. Cell* **96**,
997 639–655.

998 **Schwede, A., Manful, T., Jha, B. A., Helbig, C., Bercovich, N., Stewart, M. and Clayton, C. E.**
999 (2009). The role of deadenylation in the degradation of unstable mRNAs in
1000 trypanosomes. *Nucleic Acids Research* **37**, 5511–5528.

1001 **Shafraz, O., Davis, C. M. O. and Sivasankar, S.** (2023). Light Activated BioID (LAB): an
1002 optically activated proximity labeling system to study protein-protein interactions. *J. Cell*
1003 *Sci.* **136**, jcs261430.

1004 **Sherwin, T. and Gull, K.** (1989). Visualization of detyrosination along single microtubules
1005 reveals novel mechanisms of assembly during cytoskeletal duplication in trypanosomes.
1006 *Cell* **57**, 211–221.

1007 **Sheval, E. V., Polzikov, M. A., Olson, M. O. J. and Zatsepina, O. V.** (2005). A higher
1008 concentration of an antigen within the nucleolus may prevent its proper recognition by
1009 specific antibodies. *Eur. J. Histochem.: EJH* **49**, 117–23.

1010 **So, C., Cheng, S. and Schuh, M.** (2021). Phase Separation during Germline Development.
1011 *Trends Cell Biol.* **31**, 254–268.

1012 **Stewart, M.** (2019). Polyadenylation and nuclear export of mRNAs. *Journal of Biological*
1013 *Chemistry* **294**, 2977–2987.

1014 **Sträßer, K., Baßler, J. and Hurt, E.** (2000). Binding of the Mex67p/Mtr2p Heterodimer to
1015 Fxfg, Glfg, and Fg Repeat Nucleoporins Is Essential for Nuclear mRNA Export. *J. Cell Biol.*
1016 **150**, 695–706.

1017 **Sun, D., Fan, X., Shi, Y., Zhang, H., Huang, Z., Cheng, B., Tang, Q., Li, W., Zhu, Y., Bai, J., et**
1018 **al.** (2021). Click-ExM enables expansion microscopy for all biomolecules. *Nat. Methods*
1019 **18**, 107–113.

1020 **Sunter, J., Wickstead, B., Gull, K. and Carrington, M.** (2012). A new generation of T7 RNA
1021 polymerase-independent inducible expression plasmids for Trypanosoma brucei. *PLoS*
1022 *ONE* **7**, e35167.

1023 **Svistunova, D. M., Musinova, Y. R., Polyakov, V. Yu. and Sheval, E. V.** (2011). A Simple
1024 Method for the Immunocytochemical Detection of Proteins Inside Nuclear Structures
1025 That Are Inaccessible to Specific Antibodies. *J. Histochem. Cytochem.* **60**, 152–158.

1026 **Terry, L. J. and Wente, S. R.** (2007). Nuclear mRNA export requires specific FG nucleoporins
1027 for translocation through the nuclear pore complex. *J. Cell Biol.* **178**, 1121–1132.

1028 **Tillberg, P. W., Chen, F., Piatkevich, K. D., Zhao, Y., Yu, C.-C. (Jay), English, B. P., Gao, L.,**
1029 **Martorell, A., Suk, H.-J., Yoshida, F., et al.** (2016). Protein-retention expansion
1030 microscopy of cells and tissues labeled using standard fluorescent proteins and
1031 antibodies. *Nat. Biotechnol.* **34**, 987–992.

1032 **Tinti, M. and Ferguson, M. A. J.** (2022). Visualisation of proteome-wide ordered protein
1033 abundances in Trypanosoma brucei. *Wellcome Open Res.* **7**, 34.

1034 **Tsoi, P. S., Quan, M. D., Ferreon, J. C. and Ferreon, A. C. M.** (2023). Aggregation of
1035 Disordered Proteins Associated with Neurodegeneration. *Int. J. Mol. Sci.* **24**, 3380.

1036 **Tyanova, S., Temu, T., Sinitcyn, P., Carlson, A., Hein, M. Y., Geiger, T., Mann, M. and Cox, J.**
1037 (2016). The Perseus computational platform for comprehensive analysis of (prote)omics
1038 data. *Nature methods* **13**, 731–740.

1039 **Venko, K. and Žerovnik, E.** (2023). Protein Condensates and Protein Aggregates: In Vitro, in
1040 the Cell, and In Silico. *Front. Biosci.-Landmark* **28**, 183.

1041 **Youn, J.-Y., Dunham, W. H., Hong, S. J., Knight, J. D. R., Bashkurov, M., Chen, G. I., Bagci,**
1042 **H., Rathod, B., MacLeod, G., Eng, S. W. M., et al.** (2018). High-Density Proximity
1043 Mapping Reveals the Subcellular Organization of mRNA-Associated Granules and Bodies.
1044 *Mol. Cell* **69**, 517-532.e11.

1045 **Zatsepina, O. V., Todorov, I. T., Philipova, R. N., Krachmarov, C. P., Trendelenburg, M. F.**
1046 **and Jordan, E. G.** (1997). Cell cycle-dependent translocations of a major nucleolar
1047 phosphoprotein, B23, and some characteristics of its variants. *Eur. J. cell Biol.* **73**, 58–70.

1048 **Zhang, Y. and Shen, L.** (2023). An in vitro Assay to Probe the Formation of Biomolecular
1049 Condensates. *Bio-Protoc.* **13**, e4813.

1050

Figure 1

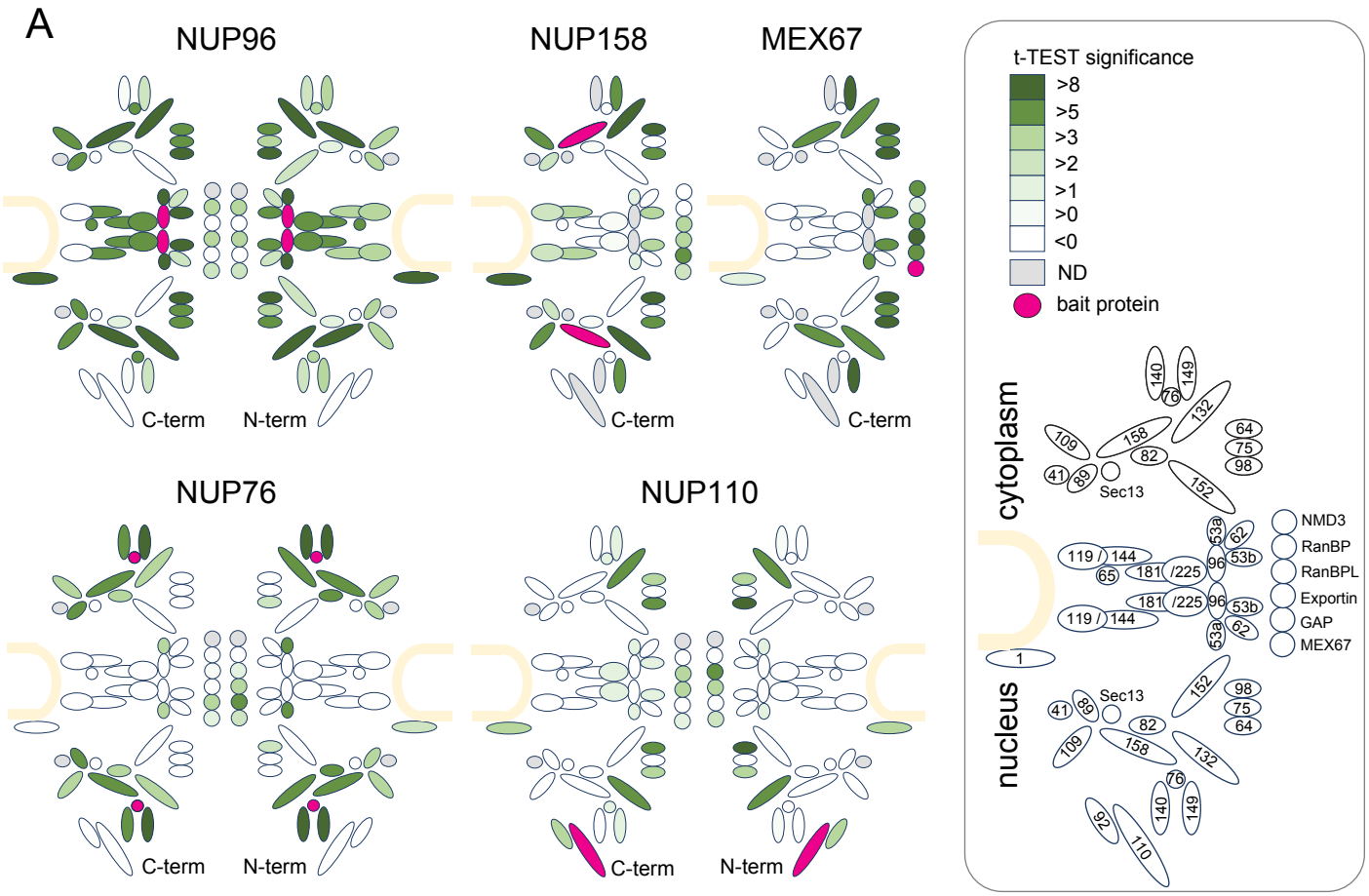
A
NUP96
NUP158
MEX67
NUP76
NUP110
C-term
N-term
t-TEST significance
>8
>5
>3
>2
>1
>0
<0
ND
bait protein
cytoplasm
nucleus
Sec13
NMD3
RanBP
RanBPL
Exportin
GAP
MEX67

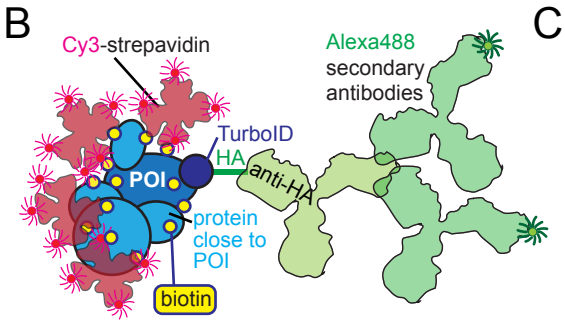
B
Cy3-strepavidin
Alexa488
secondary
antibodies
TurboID
HA
anti-HA
POI
protein
close to
POI
biotin

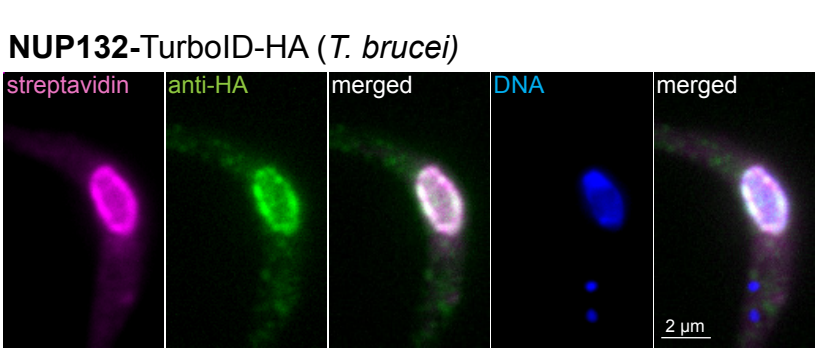
C
NUP132-TurboID-HA (T. brucei)
streptavidin
anti-HA
merged
DNA
merged
2 µm

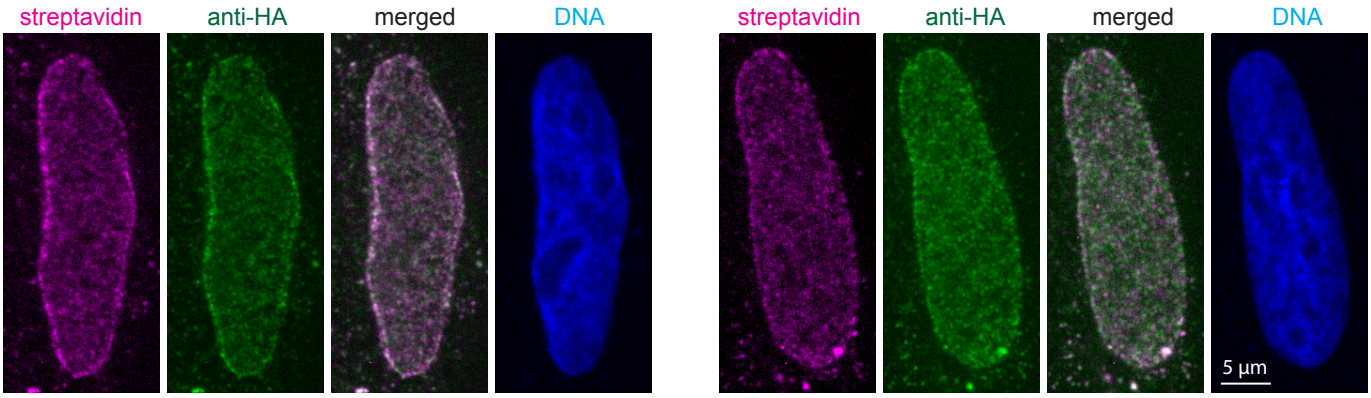
D
TurboID-4HA-NUP88 (human, HeLa)
streptavidin
anti-HA
merged
DNA
streptavidin
anti-HA
merged
DNA
5 µm

Figure 2

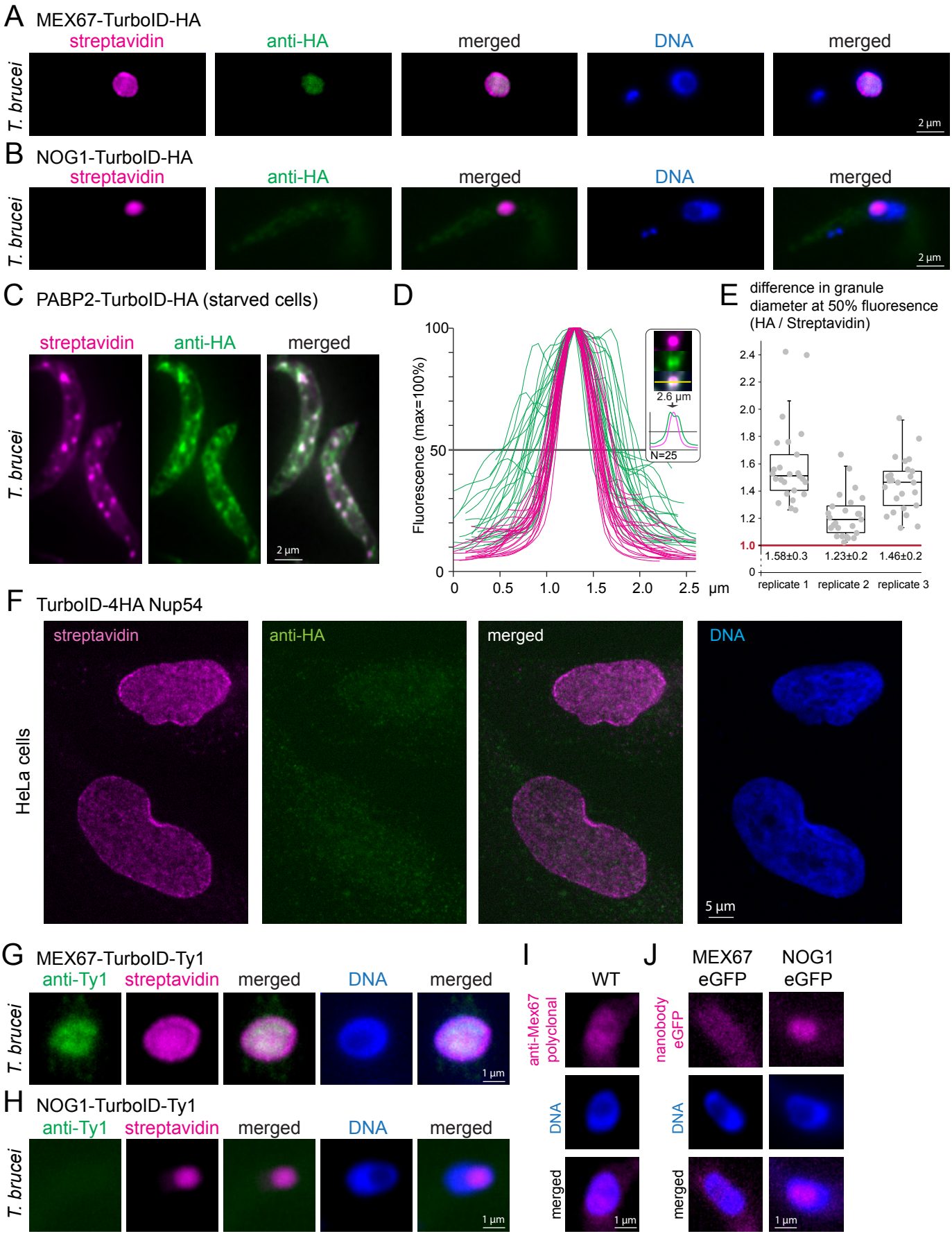
A MEX67-TurboID-HA
streptavidin
anti-HA
merged
DNA
merged
T. brucei
2 µm
B NOG1-TurboID-HA
streptavidin
anti-HA
merged
DNA
merged
T. brucei
2 µm
C PABP2-TurboID-HA (starved cells)
streptavidin
anti-HA
merged
T. brucei
2 µm
D
Fluorescence (max=100%)
100
50
0
0
0.5
1.0
1.5
2.0
2.5
µm
2.6 µm
N=25
E
difference in granule diameter at 50% fluoresence (HA / Streptavidin)
2.4
2.2
2.0
1.8
1.6
1.4
1.2
1.0
0
1.58±0.3
1.23±0.2
1.46±0.2
replicate 1
replicate 2
replicate 3
F TurboID-4HA Nup54
HeLa cells
streptavidin
anti-HA
merged
DNA
5 µm
G MEX67-TurboID-Ty1
anti-Ty1
streptavidin
merged
DNA
merged
T. brucei
1 µm
H NOG1-TurboID-Ty1
anti-Ty1
streptavidin
merged
DNA
merged
T. brucei
1 µm
I
WT
anti-Mex67 polyclonal
DNA
merged
1 µm
J
MEX67 eGFP
NOG1 eGFP
nanobody eGFP
DNA
merged
1 µm

Figure 3

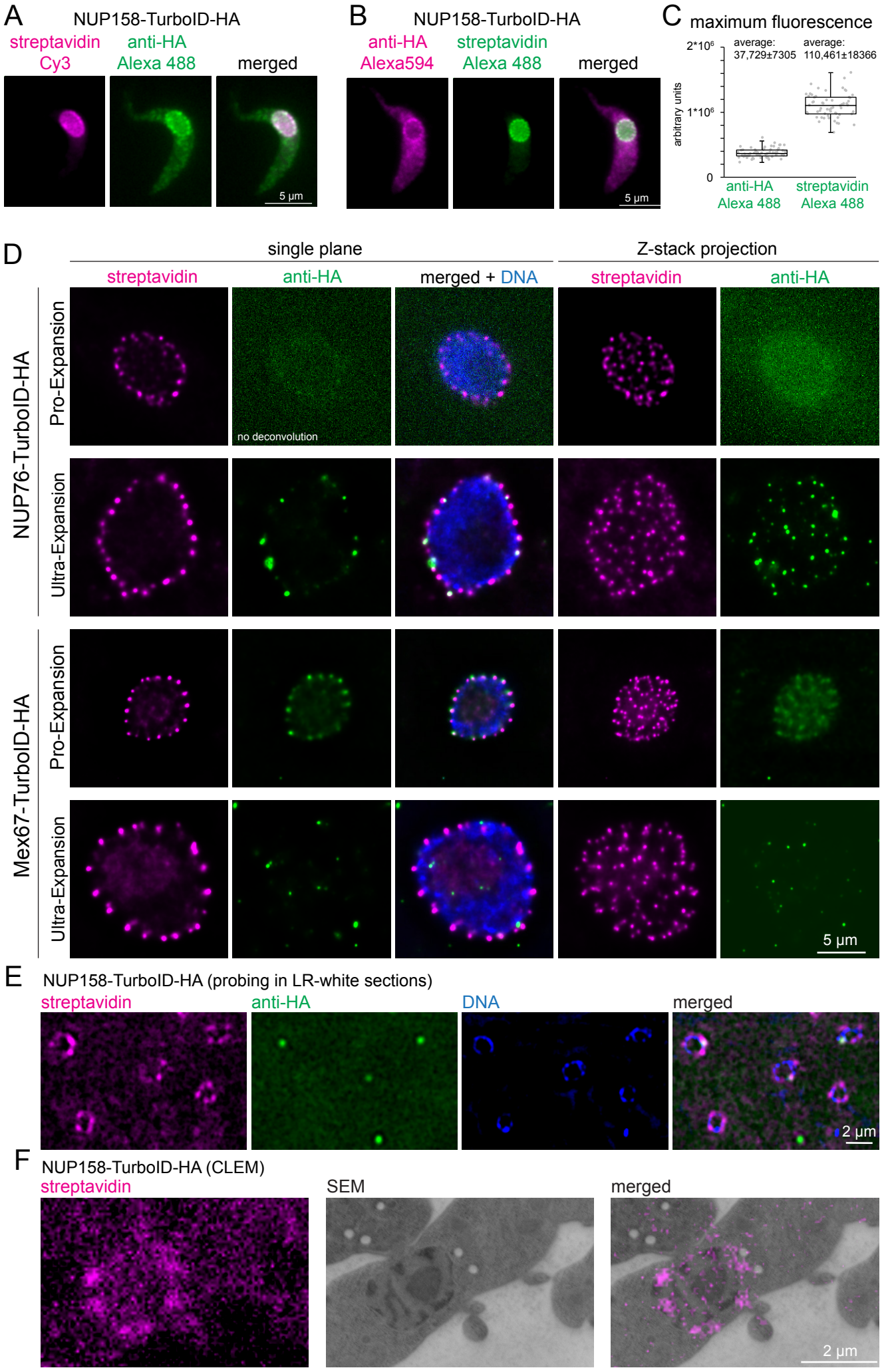
A
NUP158-TurboID-HA
streptavidin Cy3
anti-HA Alexa 488
merged
5 µm
B
NUP158-TurboID-HA
anti-HA Alexa594
streptavidin Alexa 488
merged
5 µm
C
maximum fluorescence
average: 37,729±7305
average: 110,461±18366
2*10⁶
1*10⁶
0
arbitrary units
anti-HA Alexa 488
streptavidin Alexa 488
D
single plane
Z-stack projection
streptavidin
anti-HA
merged + DNA
streptavidin
anti-HA
NUP76-TurboID-HA
Pro-Expansion
Ultra-Expansion
no deconvolution
Mex67-TurboID-HA
Pro-Expansion
Ultra-Expansion
5 µm
E
NUP158-TurboID-HA (probing in LR-white sections)
streptavidin
anti-HA
DNA
merged
2 µm
F
NUP158-TurboID-HA (CLEM)
streptavidin
SEM
merged
2 µm

Figure 4

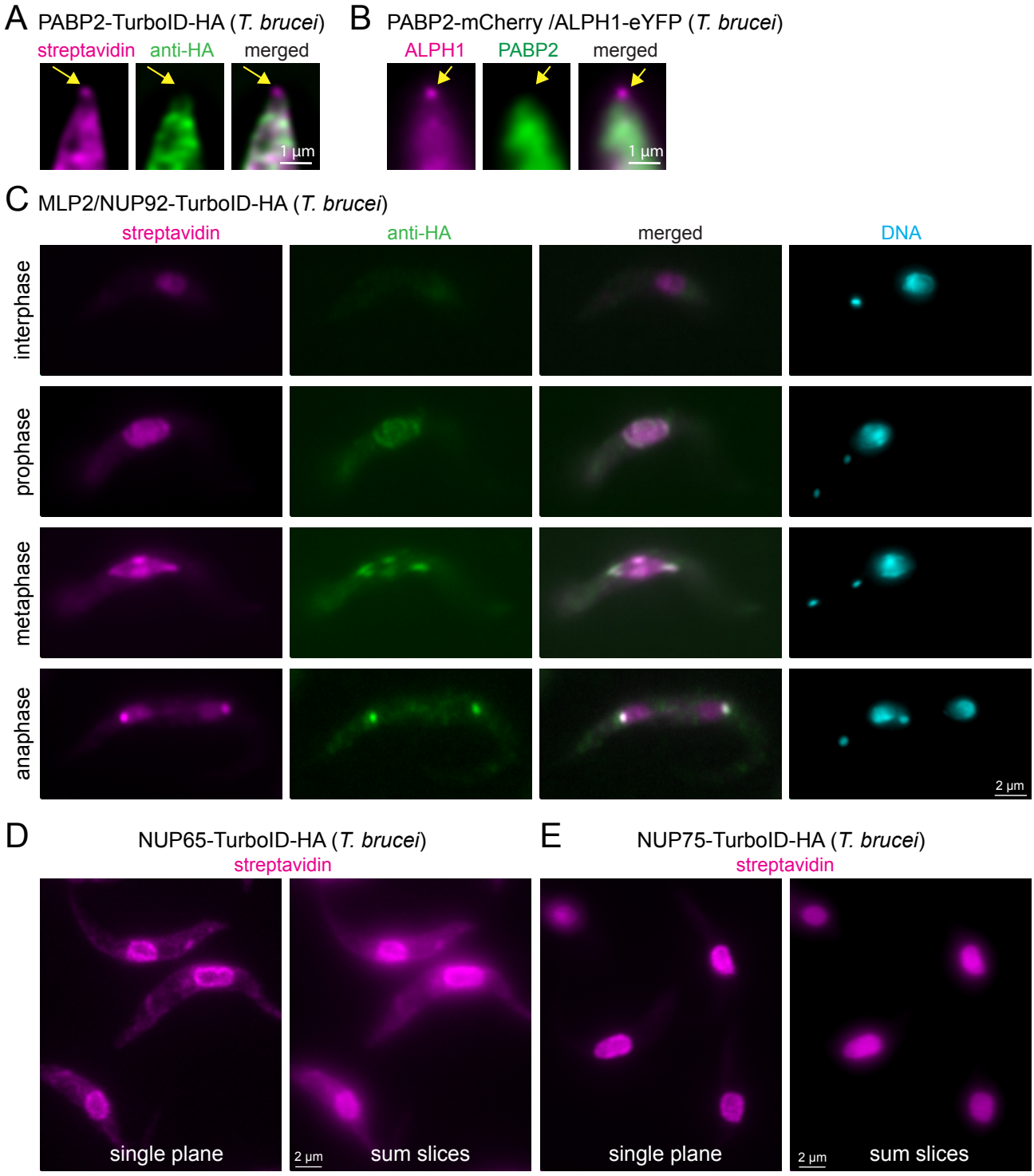
A PABP2-TurboID-HA (T. brucei)
streptavidin
anti-HA
merged
1 µm
B PABP2-mCherry /ALPH1-eYFP (T. brucei)
ALPH1
PABP2
merged
1 µm
C MLP2/NUP92-TurboID-HA (T. brucei)
streptavidin
anti-HA
merged
DNA
interphase
prophase
metaphase
anaphase
2 µm
D NUP65-TurboID-HA (T. brucei)
streptavidin
single plane
2 µm
sum slices
E NUP75-TurboID-HA (T. brucei)
streptavidin
single plane
2 µm
sum slices

Figure 5

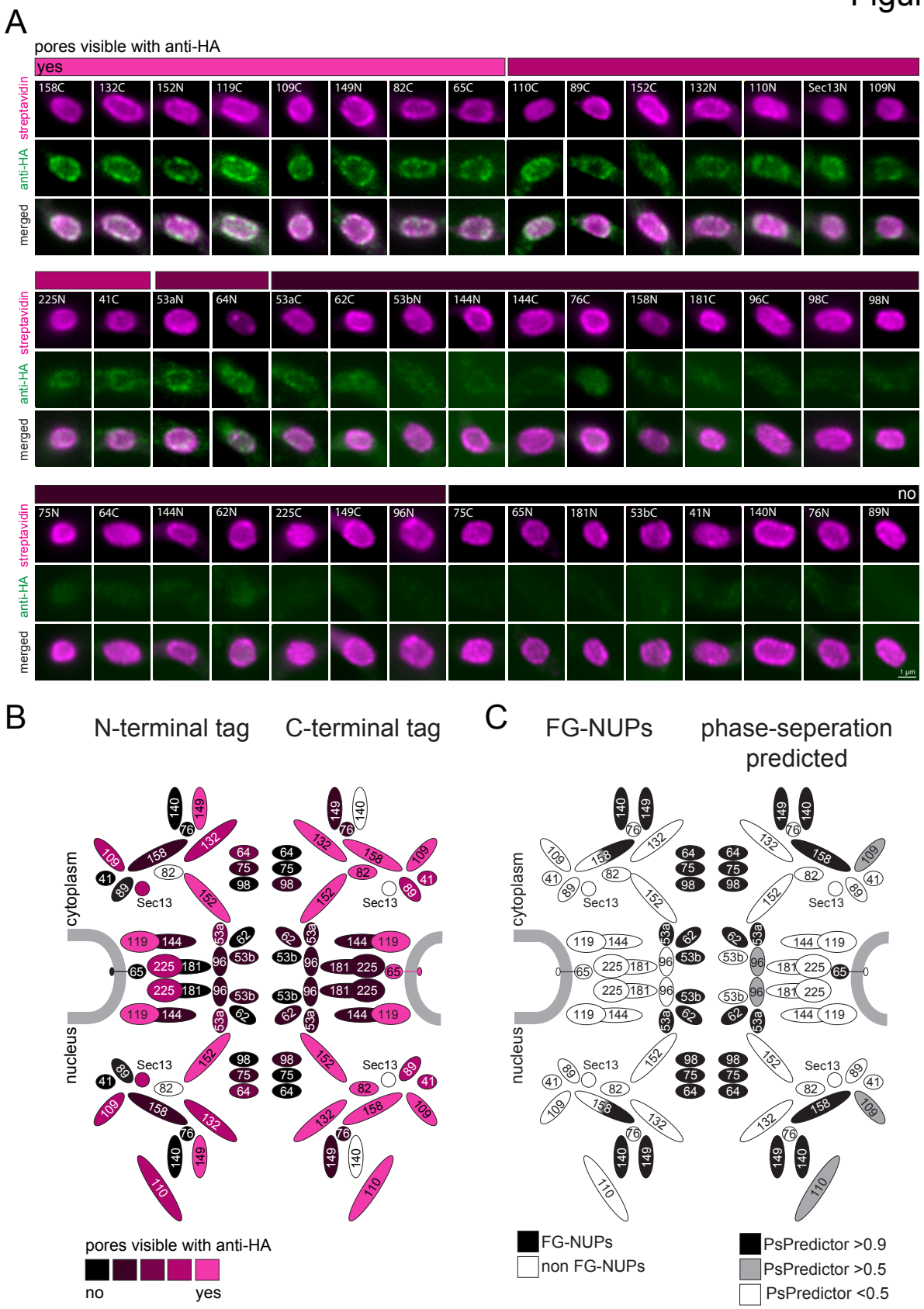
A
pores visible with anti-HA
yes
no
streptavidin
anti-HA
merged
158C
132C
152N
119C
109C
149N
82C
65C
110C
89C
152C
132N
110N
Sec13N
109N
225N
41C
53aN
64N
53aC
62C
53bN
144N
144C
76C
158N
181C
96C
98C
98N
75N
64C
144N
62N
225C
149C
96N
75C
65N
181N
53bC
41N
140N
76N
89N
1 µm
B
N-terminal tag
C-terminal tag
cytoplasm
nucleus
Sec13
pores visible with anti-HA
no
yes
C
FG-NUPs
phase-seperation predicted
FG-NUPs
non FG-NUPs
PsPredictor >0.9
PsPredictor >0.5
PsPredictor <0.5